Ice-Binding Mechanism of Winter Flounder Antifreeze Proteins

Ailan Cheng and Kenneth M. Merz, Jr.
Department of Chemistry, The Pennsylvania State University, University Park, Pennsylvania 16802 USA

ABSTRACT We have studied the winter flounder antifreeze protein (AFP) and two of its mutants using molecular dynamics simulation techniques. The simulations were performed under four conditions: in the gas phase, solvated by water, adsorbed on the ice (20$\bar{2}$1) crystal plane in the gas phase and in aqueous solution. This study provided details of the ice-binding pattern of the winter flounder AFP. Simulation results indicated that the Asp, Asn, and Thr residues in the AFP are important in ice binding and that Asn and Thr as a group bind cooperatively to the ice surface. These ice-binding residues can be collected into four distinct ice-binding regions: Asp-1/Thr-2/Asp-5, Thr-13/Asn-16, Thr-24/Asn-27, and Thr-35/Arg-37. These four regions are 11 residues apart and the repeat distance between them matches the ice lattice constant along the $\langle\bar{1}102\rangle$ direction. This match is crucial to ensure that all four groups can interact with the ice surface simultaneously, thereby, enhancing ice binding. These Asx (x = p or n)/Thr regions each form 5–6 hydrogen bonds with the ice surface: Asn forms about three hydrogen bonds with ice molecules located in the step region while Thr forms one to two hydrogen bonds with the ice molecules in the ridge of the (20$\bar{2}$1) crystal plane. Both the distance between Thr and Asn and the ordering of the two residues are crucial for effective ice binding. The proper sequence is necessary to generate a binding surface that is compatible with the ice surface topology, thus providing a perfect "host/guest" interaction that simultaneously satisfies both hydrogen bonding and van der Waals interactions. The results also show the relation among binding energy, the number of hydrogen bonds, and the activity. The activity is correlated to the binding energy, and in the case of the mutants we have studied the number of hydrogen bonds. The greater the number of the hydrogen bonds the greater the antifreeze activity. The roles van der Waals interactions and the hydrophobic effect play in ice binding are also highlighted. For the latter it is demonstrated that the surface of ice has a clathratelike structure which favors the partitioning of hydrophobic groups to the surface of ice. It is suggested that mutations that involve the deletion of hydrophobic residues (*e.g.*, the Leu residues) will provide insight into the role the hydrophobic effect plays in partitioning these peptides to the surface of ice.

INTRODUCTION

Polar fish can survive subzero temperatures during harsh winter conditions (Feeney et al., 1986; Pain, 1988; Ananthanarayanan, 1989; Davies and Hew, 1990; Feeney and Yeh, 1993; Hansen and Carpenter, 1993). Interestingly, it has been found that the freezing temperature of polar fish blood serum is lower than that of fish not adapted to the cold and that specific proteins are responsible for this freezing point depression. Thus, proteins in this class are termed antifreeze proteins (AFPs). Antifreeze glycoproteins (AFGP) are found in almost every fish living in arctic regions (DeVries et al., 1970). AFP are believed to bind to ice surfaces and to inhibit ice crystal growth, thereby lowering the freezing point of the body fluids of fish (Ananthanarayanan, 1989; Feeney and Yeh, 1993; Yeh and Feeney, 1996).

The study of the binding mechanism(s) of AF(G)Ps to ice surfaces is of great importance to a broad range of research fields and potentially has numerous practical applications. For example, it can stimulate a deeper understanding of crystal growth (Raymond and DeVries, 1977; Knight et al., 1984; Kerr et al., 1987); it is relevant to the interaction between proteins and surfaces (such as membranes) in general (Hays et al., 1993), and it is crucial to cryopreservation research since ice crystal growth can significantly damage cryopreserved biological materials (Arav et al., 1993). Thus, adding an AF(G)P to a protectant solution can inhibit ice crystal growth and therefore reduce damage due to ice crystal growth. Further practical applications include prevention of damage to agricultural crops by early frost (Kenward et al., 1993) and inhibition of ice crystal growth in foods stored at low temperatures (Feeney and Yeh, 1993). The study of AF(G)Ps is also of great significance to fish and marine life physiology and in increasing our ability to farm fish in cold conditions by genetic incorporation of AFPs into fish from temperate regions (Burcham et al., 1984). Thus, AF(G)Ps have drawn the attention of scientists in many fields.

The best-studied AFP is winter flounder HPLC-6 AFP (one of two major components has been isolated by HPLC methods, the other major component is labeled HPLC-8) (Ananthanarayanan, 1989; Yeh and Feeney, 1996). X-ray studies suggest that this alanine-rich type I AFP is an α-helix with four threonine residues on one side that, presumably, bind to the ice surface through hydrogen bonding (Yang et al., 1988). Chakrabartty et al. have examined the role of charged amino acids on the stability of the α-helix of this AFP (Chakrabartty et al., 1989a,b). Knight et al. (1991), using crystal growth and etching techniques, determined that the winter flounder AFP adsorbed onto the {20$\bar{2}$1}

Received for publication 27 January 1997 and in final form 2 September 1997.

Address reprint requests to Dr. Kenneth M. Merz, Jr., Dept. of Chemistry, Pennsylvania State University, 152 Davey Lab, University Park, PA 16802-2801. Tel.: 814-865-3623; Fax: 814-863-8403; E-mail: merz@retina.chem.psu.edu.

0006-3495/97/12/2851/23 $2.00

pyramidal planes of ice and is probably aligned along the [01$\bar{1}$2] direction. The repeat distance of the Thr residues along the α-helix nearly matches the ice lattice spacing along the [01$\bar{1}$2] direction. It is believed that this structural match is important in the ice-binding properties of type I AFPs. Studies by Wen and Laursen supported this model and suggested that the binding is unidirectional and ice growth inhibition occurs by a two-step process (Wen and Laursen, 1992a,b; 1993). A recent x-ray crystal structure study by Sicheri and Yang (1995) provided more detailed structural information and lead to a proposed ice-binding motif.

Several theoretical studies have been reported on winter flounder HPLC-6 AFPs. The energy minimization study by Chou (1992) examined the Thr repeat distance and the results agree with experimental studies to some extent. A molecular dynamics simulation study by Jorgensen et al. (1993) also suggested that the evenly spaced Thr residues play an important role in ice binding. They have found that the charged residues stay on the opposite side of the helix and do not participate in ice binding. Lal et al. (1993) studied the *in vacuo* binding energy of the AFP with different surfaces using a docking procedure and energy minimization method. The results showed that AFP has a higher affinity for the {20$\bar{2}$1} plane than for the c and prism faces. McDonald et al. (1993) studied the winter flounder AFP both in vacuum and in solution using a united atom potential model and examined the possible causes for the observed bending of the α-helix in their simulations. Madura et al. (1994) have reported a preliminary study of the D- and L-form of winter flounder AFP on ice surfaces using energy minimization methods.

We have studied the winter flounder AFP and two mutants in vacuum, in aqueous solution, and adsorbed on ice surfaces in the gas phase and in aqueous solution using an all-atom potential model by molecular dynamics (MD) simulations over long simulation time scales in order to shed some light on the ice-binding mechanism of AFP. This is the most detailed modeling study to date and addresses the roles hydrogen bonding, as well as van der Waals (hydrophobic effect) interaction, play in the ice-binding properties of these unique peptides. The results from these studies are described in detail below.

SIMULATION DETAILS

We have carried out several sets of simulations: winter flounder AFP in vacuum, in water, and adsorbed on an ice surface in the gas phase and in aqueous solution. We have also examined two mutants of the winter flounder AFP in the gas and neat adsorbed phases. The peptide studied here has 37 residues with 11 residue repeats. The primary sequence is:

```
Asp-Thr-Ala-Ser-Asp-Ala-Ala-Ala-Ala-Ala-Ala-Leu-
    Thr-Ala-Ala-Asn-Ala-Lys-Ala-Ala-Ala-Glu-Leu-
    Thr-Ala-Ala-Asn-Ala-Ala-Ala-Ala-Ala-Ala-Ala-
    Thr-Ala-Arg
```

The state of the C-terminus in the HPLC-8 AFP has been suggested to be amidated based on electrophoretic data (Hew et al., 1986) and by inference it has been suggested that HPLC-6 AFP is also amidated at the C-terminus. Based on this one piece of data the crystal structure of these peptides are also given as amidated (Sicheri and Yang, 1995). Previous modeling studies of the HPLC-6 AFP have treated the N- and C-termini as neutral, charged, or amidated. In this study we treat these peptides as zwitterions, and given that we are mostly interested in the inner regions of the peptides, we expect that whether we treat the terminal regions as neutral or charged (or the C-terminus as amidated) will have little effect on this region of the ice/AFP binding interaction. In the case where the C-terminus is a carboxylate, Chakrabartty et al. (1989a) have shown that the AFP is a zwitterion.

The AMBER all-atom force field for proteins (Weiner et al., 1984) and the TIP3P (Jorgensen et al., 1983) potential model for liquid and ice water molecules, and the molecular dynamics simulation package AMBER 4.0 (MINMD), were used (Pearlman et al., 1991). The time step used was 1 fs and the pair list was updated every 25 steps. The cutoff distance was set to 12 Å for the gas phase simulation and 9 Å for the solvated and adsorbed phase simulations. The SHAKE algorithm was used to constrain all X-H bonds to their equilibrium values with a tolerance of 0.0004 (Ryckaert et al., 1977). Periodic boundary conditions and the minimum image convention were adopted in the aqueous phase simulations. All simulations were performed at a constant temperature (300 K) using Berendsen's algorithm with a temperature coupling constant of τ_T = 0.2 ps (Berendsen et al., 1984). In order to better sample phase space we have simulated these systems at 300 K rather than 273 K. This is an approach that has been utilized by others in the past (e.g., protein unfolding studies) and is justified in that we want to sample as much of the relevant phase space as possible, and clearly at 273 K very little phase space would be sampled even over many nanoseconds of simulation.

The starting configurations for the MD simulations were prepared in the following way: experimental studies indicated that the winter flounder AFP adopts an α-helical structure at ambient conditions (Yang et al., 1988), however, when we began this work no experimental structure was available (Sicheri and Yang, 1995). Since it was expected that there would be little structural variation for a regular α-helix, we built an α-helix model for the AFP to start our simulations. When the x-ray structure became available (Sicheri and Yang, 1995) we compared our structure to this structure. We matched the coordinates of the heavy atoms in our structure with each of the two structures obtained from x-ray studies (each has two molecules per unit cell) and found that the RMS deviations between our structure and the experimental structures (RMS deviations of ~1.9) are nearly the same as that between the two x-ray structures themselves (RMS deviations between 0.7–1.9). Moreover, we find in our MD simulations that we observe a 1.9 Å RMS deviation between our starting structure and

the structure obtained after 200 ps. Thus, we feel that an RMS deviation of ~2.0 is within the thermal fluctuations of this system. In this manner we determined that our starting structure was a suitable model for the α-helical AFP. Next, 200 cycles of energy minimization using steepest descent, followed by 10,000 cycles using the conjugated gradient method, were performed. The last configuration was taken as the initial configuration for the simulation of the AFP in the gas phase. The first 400 ps of this simulation was discarded and then a 200-ps trajectory was collected and stored for analysis.

The second simulation was performed for the AFP solvated by water at the same temperature (300 K) in order to examine the interactions between the AFP and liquid water. The AFP with the same structure as that used in the previous gas-phase simulation was solvated by a box of water taken from an equilibrated Monte Carlo simulation. Any water molecule with its oxygen atom within 1.9 Å and its hydrogen atoms within 0.8 Å of any AFP atom was discarded to avoid close water/peptide contacts. The resultant simulation cell contained 1130 water molecules. Five hundred cycles of energy minimization were performed to further eliminate any close water/peptide contacts. A constant pressure simulation using the Berendsen method (Berendsen et al., 1984) was carried out for 20 ps to allow the system to relax to the proper density. The resulting simulation cell had the dimensions of 66.86 Å × 25.05 Å × 22.83 Å. The final configuration from this run was taken to be the starting configuration of the solvated phase simulation performed at constant volume and temperature. The system was equilibrated for 200 ps and the next 200 ps of trajectory was saved for data analysis.

The third simulation involved an AFP adsorbed on the surface of a slab of ice. The ice was assumed to have the crystal structure of ordinary ice (I_h). The oxygen positions of the ice I_h phase belong to the space group denoted by the Schoenflies symbol D_{6h}^4 or by the international symbol P_{63}/mmc (Wyckoff, 1969). The tetramolecular hexagonal unit of ordinary ice has the edges a_0 = 4.5227 Å, c_0 = 7.3671 Å at 0°C with the oxygen atoms located at ±(⅓, ⅔, u; ⅔, ⅓, u + ½), where u = 1/16. The water orientations were randomized first, then 10 ps of simulation using the TIP3P potential model was performed to optimize the water orientations while the oxygen atoms were held fixed. The crystal growth and etching experiments suggested that the winter flounder AFPs bind to the ice {20$\bar{2}$1} surface and prefer to align along [01$\bar{1}$2] direction. There exist 12 equivalent {20$\bar{2}$1} planes and 12 equivalent [01$\bar{1}$2] directions. We chose to study the AFP adsorbed on a specific plane denoted by (20$\bar{2}$1) which has the corresponding specific direction of ⟨$\bar{1}$102⟩. The reference x axis was chosen to be along the ⟨$\bar{1}$102⟩ direction and the z axis is along the norm of the surface. Given that the surface orientation of AFPs are known we did not exhaustively search for binding on other surfaces and orientations of ice. Instead we focused on the known orientation in order to better understand how these peptides bind to model ice surfaces.

The ice surface consists of 1500 water molecules packed in 15 layers. The surface is almost square with dimensions 83.436 Å × 82.642 Å, which is much larger than the length of the α-helix (~50 Å), which will minimize artifacts arising due to edge effects. The final ice slab was 7.1 Å thick.

The last conformation of the AFP from the gas phase simulation was taken as the initial configuration for the AFP on ice. The AFP was moved along the norm of the surface to map out the binding energy profile while the helix was held rigid and parallel to the surface. Then the center of mass of the helix was placed at the distance which gave a minimum in the binding energy. This configuration was taken as the starting configuration for the simulation of the adsorbed system. During the simulation the center of mass of the water molecules were held fixed, allowing the water molecules to freely rotate, since surface melting and surface reconstruction may occur which would complicate the simulation, while concomitantly interfering with our desire to address the biological question of how these peptides interact with a model ice surface. The system was equilibrated for 350 ps. Then a trajectory covering 200 ps was saved for data analysis. All simulations were done at 300 K to ensure that the ice surface was thoroughly sampled by the AFP.

In order to prepare for the simulation of the AFP adsorbed on ice surrounded by aqueous solution, we trimmed the ice surface of the previous run (66.748 Å × 37.189 Å with 540 ice molecules) in order to reduce the computational expense. Here, periodic boundary conditions were employed, thus, the AFP/ice system was solvated by water only along the z direction in order to maintain the periodicity of ice lattice along the x-y plane. The ice slab was centered along the z axis. The x-y dimensions are large enough such that the AFP does not directly interact with its image given the cutoff distance used (9 Å). The resulting box had 1917 liquid water molecules and was 39.176 Å along the z direction. The z direction of the box was allowed to relax for 10 ps by carrying out a constant pressure simulation while holding the AFP and ice atoms fixed. The final box dimensions were 66.748 Å × 37.189 Å × 32.378 Å. The final configuration of this run was taken as the initial configuration for the simulation of AFP/ice/water simulation. The simulation was run at 300 K and was equilibrated for 350 ps followed by a trajectory covering 200 ps. During these simulations we again restrained the center of mass of the ice molecules partly because we were only interested in the effect solvent water molecules had on AFP/ice binding. In addition, accurately modeling an ice/water interface is a difficult problem. Indeed, there is not a sharp boundary between the solid and liquid phases in the interfacial region. The typical interface thickness is a macroscopic quantity by molecular dynamics simulation standards. As shown in the work of Karim and Haymet (1988), slabs of rather large sizes (106 and 147 Å along the z direction) were required to accurately simulate an ice/water interface. If the peptide is placed in the interface region, and in order to avoid the interaction of peptide with its images, a much large surface than this would be required to model our water/AFP/ice

interface at the same level of sophistication. Thus, in order to have a system with a reasonable size, we chose a thin interface where we have fixed the center of mass of a fraction of the water molecules, which we have characterized as ice.

The simulation results of the above-mentioned four systems indicated that the behavior of the native peptide showed great similarity between the neat adsorbed phase (i.e., ice only) and when adsorbed on the ice/water interface (see below). Thus, we have studied the two mutants of the winter flounder AFP only in the gas and adsorbed phases to reduce the computational expense. Many different mutations are possible; however, we were only interested in the modification of two of the Thr/Asn groups. Here, we have chosen the two mutants synthesized by Wen and Laursen (1992a,b) because their activities are well characterized. These two mutants have activities of 0.65 and 0.17 relative to that of the native AFP, and are labeled herein as S11 and S23 as was done in the original experimental papers (Wen and Laursen, 1992a,b). Wen and Laursen have also estimated the number of hydrogen bonds formed between AFP mutants and ice surfaces using energy minimization methods (Wen and Laursen, 1992a). The two Thr/Asn mutants we have studied have the same amino acids as in the native one, but the sequence is permuted. The mutant labeled S11 has identical sequence as the native one except the interchange of Asn-27 and Ala-30. Mutant S23 has two modifications relative to the native sequence: interchange of Asn-27 and Ala-30 and the interchange of Thr-13 and Asn-16.

The last configurations of the gas phase and the adsorbed phase of the native peptide were used to generate the initial configurations for the simulations of the mutants in order to minimize any artifacts due to the choice of the initial configurations. Thus, the starting configurations for the mutants maintain the same orientation as that of the native peptide. The coordinates of all the atoms were kept the same except for those atoms in the side chains of the mutated residues. The side-chain configurations of those mutated residues were taken from the standard AMBER database and the resulting structures were energy minimized to eliminate any unfavorable contacts. The trajectories for the first 400 ps for the gas phase and the first 800 ps for the adsorbed phase were discarded. Then trajectories covering the following 200 ps were saved for further analysis.

SIMULATION RESULTS

In an effort to better understand the ice-binding mechanism of the AFP, we compared the structure and interactions of the AFP with its environment under four different conditions. All four simulations covered reasonably long simulation time scales to ensure that the systems were well-equilibrated. The thermodynamic properties such as temperature, configurational energy, and total energy indicated that the systems had reached equilibrium rather rapidly and that the trajectories were collected after the systems were well-equilibrated. The average temperature for the simulations of native peptide in the gas phase, solvated phase, and adsorbed phases without and with aqueous water are 300.0, 306.4, 304.2, and 304.9 K, respectively. The resulting simulation temperatures for the two mutants were 300 K for the gas phase and 304 K for the adsorbed phase simulations. These values are close to the desired value of 300 K. The slightly higher temperatures for the latter three runs were due to artifacts of the simulation algorithm and this has been discussed in detail elsewhere (Cheng and Merz, 1996). In this section we present the results of the four simulations. The results are presented in two distinct sections: AFP structure and AFP-water interactions.

AFP structure

Backbone structure

The conformation of the backbone of the α-helix AFP can be described by the dihedral angles formed by four consecutive atoms. The two dihedral angles often used for peptides are ϕ (C-N-C_α-C) and ψ (N-C_α-C-N). The average values for these dihedral angles and their root-mean-square fluctuations were evaluated for each residue in the four simulations. They are shown in Fig. 1. The average values for the dihedral angles are very close to that of an ideal α-helix, $\phi = -57°$ and $\psi = -47°$. The fluctuation is typically 8–9° for those residues away from the termini of the α-helix. The two residues at each terminus exhibit more torsional flexibility since there are no neighboring residues to interact with. The helix bends somewhat in the AFP/ice/water simulation. Thus, the average values for the torsion angles for residue 27 were $\phi = -23°$ and $\psi = -70°$, and each had a slightly higher fluctuation of 13–14°. We define the helicity as the probability for both ϕ and ψ staying within 15° of the ideal α-helix torsion angles. These values are estimated for each residue and are presented in Fig. 2. Again, the residues at the ends show little or no helical content and those in the middle maintain >80% helicity during the 200-ps trajectory. The slight dip at Lys-18 for the gas phase and at Glu-22 for the solvated phase is related to the bending of the peptide backbone, which was discussed in detail by McDonald et al. (1993). For the AFP/ice/water run, bending causes the torsion angles at residue 27 to be ~35° away from the ideal α-helix angles, thus, the helical content in this region drops dramatically. The mutants maintain an α-helical conformation for >80% of the simulation time again except at the two ends where fraying was observed. If 20° is used as the criterion in the helicity calculation, the helix content would be >95% for all simulations.

Side chain conformations

In addition to the backbone dihedral angles, the side chain conformation is needed to give a complete description of the peptide structure. Thus, the side chain dihedral angles were

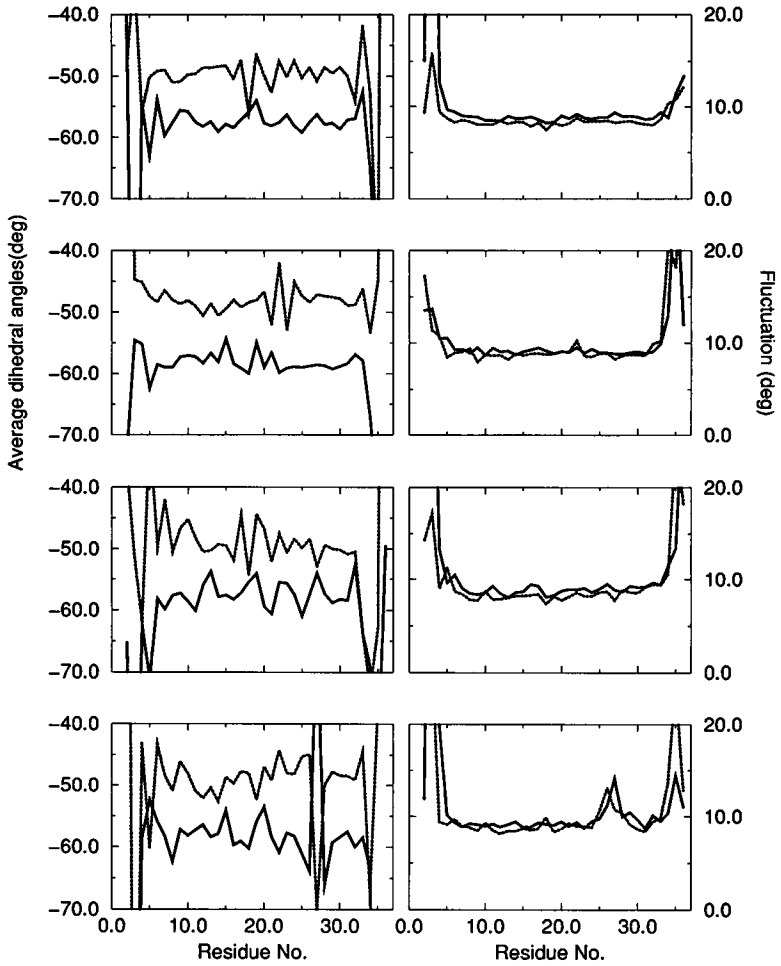

FIGURE 1 The average backbone dihedral angles, ϕ (*solid line*) and ψ (*dotted line*), for each residue of the AFP in the four simulations. From top to bottom we have the gas, solvated, AFP/ice, and AFP/ice/water phases, respectively. The figures on the right side show the corresponding root-mean square fluctuations.

studied and they are defined as χ_1 (N-C_α-C_β-X), χ_2 (C_α-C_β-X1-X2), etc., down the side chain, respectively. Only angles involving four heavy atoms (i.e., nonhydrogen atoms) were examined, which means alanine residues are not included in this discussion. The average torsion angles and the root-mean-square fluctuations are shown in Tables 1–4 for the four sets of simulations, respectively.

In all four simulations the side chain torsion angles of those residues away from the two termini of the helix display some characteristic features. There were very few *gauche*$^+$ angles for χ_1 since that conformation would cause the side chain to clash with the backbone atoms of the previous turn of the α-helix. The β-branched Thr side chains were found to be very restricted due to steric considerations. For example, the side chain torsion angles for Thr-13 and Thr-24 show fluctuations that are typically $<10°$. For the Thr residues note that χ_1 and χ_2 represent the torsion angles involving -CH_3 and -OH groups, respectively. The fluctuation for the two angles are very similar in value since they are correlated to maintain the tetrahedral geometry around C_β. In fact, the two angles have similar values ($\chi_1 = -170°$ and $\chi_2 = -50°$) for all four simulations. This suggests that these two Thr residues hydrogen-bond to the backbone or other AFP atoms in a similar way for all four runs. Interestingly, the side chain torsion angles χ_1 and χ_2 for Thr-2 and Thr-35 give slightly higher fluctuations. The values for these torsion angles vary among the four simulations, which suggests different hydrogen bonding patterns for these Thr residues at the two ends of the α-helix. The details of the hydrogen bonding patterns for the Thr residues will be discussed later. The -OH group of Ser-4 was observed to be very rigid, especially for the gas and adsorbed phases. The average values of χ_1 for the four simulations were $-44°$, $-28°$, $-40°$, and $-42°$ with small fluctuations of 9°, 39°, 9°, and 16°, respectively. The slightly different torsion angle ($-28°$) for the aqueous phase simulation may be related to the fact that Ser-4 forms hydrogen bonds with the surrounding water molecules.

The fluctuations in the side chain torsion angles for Asn-16 and Asn-27 were found to be higher in the gas and solvated phases than in the adsorbed phases where the side chains of Asn-16 and Asn-27 were hydrogen-bonded to the ice surface. For example, the two torsion angles χ_2 and χ_3, which represent the side chain oxygen and nitrogen atoms, respectively, showed this behavior. This same behavior is also seen for Asp-1 and, to a lesser extent, for Asp-5. This is due to hydrogen bonding between the carboxylate oxy-

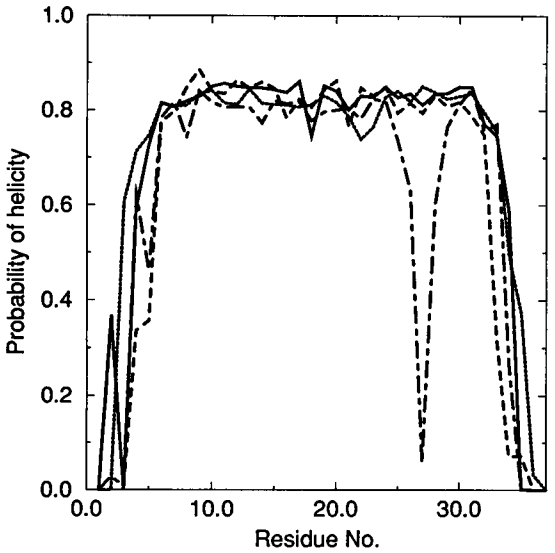

FIGURE 2 The probability of the backbone dihedral angles staying within 15° of the ideal α-helix angles for the AFP in the gas (*solid line*), solvated (*dotted line*), AFP/ice (*dashed line*), and AFP/ice/water (*dotted-dashed line*) phases.

gens and the ice surface. More details regarding these interactions are given below.

Finally, for the native peptide, we note that the γ-branched hydrophobic residues Leu-12 and Leu-23 show relatively great torsional flexibility in the gas, solvated, and "neat" adsorbed phase. The flexibility was reduced significantly when the AFP was placed at the ice/water interface. This is likely due to the steric constraints imposed by both the surrounding water and the ice surface.

The side chain conformations observed for the mutants and the native peptide were similar in the gas phase. For the adsorbed phase the side chain configurations near the mutated residues differ from the native one while that of the preserved residues remain essentially the same. The average torsion angles and the root-mean-square fluctuations of some residues are shown in Tables 5 and 6 for the two mutants compared to that for the native protein in Tables 1 and 3. For the Thr residues, the $-CH_3$ and -OH groups are represented by χ_1 and χ_2, respectively. For the Asn residues the angles χ_2 and χ_3 represent the side chain carbonyl oxygen and amine groups, respectively. The torsion angles for the residues Ser-4, Lys-18, Glu-22, Leu-12, and Leu-23 in the two mutants behave similarly to those of the native peptide in the gas and adsorbed phase and, therefore, are not shown in the tables. The side chain torsion angles of Asp-1, Asp-5, and Arg-37 vary slightly among the different systems due to the rearrangement of the C- and N-terminus hydrogen bond networks. However, it seems that the changes can be ascribed to thermal fluctuations rather than to the point mutations.

The side chains of most of the Thr residues maintain the torsional preference observed in the native peptide except for that of Thr-16 in the S23 (recall, Asn-27/Ala-30 and Thr-13/Asn-16 interchange) mutant. When S23 is adsorbed on the ice surface, the side chain of Thr-16 adopts a different conformation in response to a change in the hydrogen bonding pattern. The torsional fluctuations of Asn-16 in the native protein and those in the mutated position Asn-13 were found to be reduced significantly upon adsorption when compared to the gas phase. Asn-27 in the native peptide shows reduced torsional flexibility when adsorbed on ice via hydrogen bonding interactions. However, the torsion angle fluctuation of Asn-30 in the two mutants is similar to that observed in the gas phase and, therefore, is significantly greater than that of Asn-27 in the native peptide in the adsorbed phase. This indicates that Asn-30 in the mutants does not form long-lived hydrogen bonds with the surface ice molecules. It will be shown later that the changes in side chain conformations are closely related to changes in ice-binding patterns due to the site-specific mutations.

TABLE 1 The side chain dihedral angles and their root-mean-square fluctuations for the AFP in the gas phase

	χ_1	χ_2	χ_3	χ_4	χ_5	χ_6
Residue						
Asp-1	120	−91	78			
Thr-2	−133	−13				
Ser-4	−44					
Asp-5	55	−165	8			
Leu-12	−97	154	−85			
Thr-13	−171	−52				
Asn-16	174	148	−32			
Lys-18	−173	−168	115	17		
Glu-22	−69	168	−31	156		
Leu-23	−174	85	−153			
Thr-24	−171	−51				
Asn-27	174	133	−48			
Thr-35	−68	54				
Arg-37	42	80	−66	−69	−23	156
Fluctuations						
Asp-1	52	29	29			
Thr-2	28	27				
Ser-4	9					
Asp-5	8	14	16			
Leu-12	46	37	38			
Thr-13	9	9				
Asn-16	13	81	81			
Lys-18	14	24	58	58		
Glu-22	8	9	21	19		
Leu-23	20	41	41			
Thr-24	9	9				
Asn-27	13	78	78			
Thr-35	8	8				
Arg-37	8	7	8	9	8.0	8

Hydrogen bonding

Here, we examine the hydrogen bond interactions that play an important role in protein/protein and protein/surface interactions. In this section we briefly focus on the intrapeptide hydrogen bonds in the four simulations. The criterion of forming a hydrogen bond is purely according to the donor and acceptor geometry (Tirado-Rives and Jorgensen, 1990).

TABLE 2 The side-chain dihedral angles and their root-mean-square fluctuations for the AFP in the aqueous phase

	χ_1	χ_2	χ_3	χ_4	χ_5	χ_6
Residue						
Asp-1	180	99	−142			
Thr-2	−164	−44				
Ser-4	−28					
Asp-5	178	−106	75			
Leu-12	−97	167	−72			
Thr-13	−170	−50				
Asn-16	174	−14	166			
Lys-18	−69	−178	−19	178		
Glu-22	−64	−115	131	−49		
Leu-23	−155	112	−127			
Thr-24	−103	17				
Asn-27	176	−21	159			
Thr-35	−159	−39				
Arg-37	−66	−179	180	−180	0	−180
Fluctuations						
Asp-1	10	72	72			
Thr-2	10	11				
Ser-4	39					
Asp-5	10	20	20			
Leu-12	46	13	14			
Thr-13	10	10				
Asn-16	14	92	92			
Lys-18	9	13	64	14		
Glu-22	10	47	61	62		
Leu-23	45	52	52			
Thr-24	44	45				
Asn-27	10	88	88			
Thr-35	26	26				
Arg-37	11	12	13	22	12	12

TABLE 3 The side-chain dihedral angles and their root-mean-square fluctuations for the AFP adsorbed on ice

	χ_1	χ_2	χ_3	χ_4	χ_5	χ_6
Residue						
Asp-1	65	112	−60			
Thr-2	−124	−4				
Ser-4	−40					
Asp-5	92	−59	125			
Leu-12	−130	118	−120			
Thr-13	−174	−53				
Asn-16	158	−123	56			
Lys-18	−164	−175	66	58		
Glu-22	−70	166	151	−37		
Leu-23	−168	96	−143			
Thr-24	−171	−51				
Asn-27	168	79	−102			
Thr-35	−83	36				
Arg-37	−80	76	−83	179	3	−177
Fluctuations						
Asp-1	6	8	8			
Thr-2	41	40				
Ser-4	9					
Asp-5	16	11	11			
Leu-12	55	54	54			
Thr-13	8	7				
Asn-16	9	14	14			
Lys-18	11	8	12	9		
Glu-22	8	8	15	16		
Leu-23	31	46	46			
Thr-24	8	8				
Asn-27	9	13	13			
Thr-35	22	22				
Arg-37	11	12	11	12	11	10

If the H-acceptor distance was <2.5 Å and the donor-H-acceptor angle was >120°, we considered that a hydrogen bond was present. Using this criterion all possible hydrogen bonds were examined. The probability, the average bond length, and donor-H-acceptor angle were determined for each hydrogen bond. The hydrogen bonds were separated into two groups. The first group included those formed by the backbone carbonyl oxygen and the backbone amide hydrogen of the fourth residue along the helix, herein denoted as the (i, i + 4) hydrogen bond. The existence of this type of hydrogen bond is one of the conspicuous features of α-helices. The second group consisted of hydrogen bonds formed between any hydrogen and acceptor atoms on the side chains of all the residues. This second group also includes those hydrogen bonds formed between hydrogen atoms on the side chains and acceptors on the backbone.

The probabilities, the hydrogen bond lengths, and angles of the 33 possible backbone (i, i + 4) hydrogen bonds were determined for the four simulations. In most cases the average hydrogen bond distance is between 1.9 and 2.1 Å and the average donor-H-acceptor angle is between 155 and 165°. For the solution and surface bound simulations the probability of forming an (i, i + 4) hydrogen bond was >90% except for the terminal residues that were frayed and had probabilities <90%. The probabilities for the gas phase simulation were almost 99% for all backbone hydrogen bonds which indicates, not unexpectedly, that the helix is rather stable in the gas phase. In all cases a slightly lower value for the hydrogen bond between Ala-17 and Ala-21 was observed and is probably related to the bending of the helix observed in this region. For the AFP adsorbed with liquid water the bending occurs around residues 26 and 27; thus, the two hydrogen bonds between the carbonyl O of Thr-24 and the amide HN of Ala-28, and the carbonyl O of Ala-25 and amide HN of Ala-29, were broken during the entire length of the simulation. At the C-terminal end of the peptide the carboxylate oxygen atoms tend to hydrogen-bond to the amide hydrogen of the second, third, or fifth residues instead of fourth residue, while the amide hydrogen atoms of the N-terminal region tend to hydrogen-bond to the side chain oxygen of Asp-1.

Polar hydrogens on the side chains can hydrogen-bond to acceptors on adjacent side chains or with the backbone of the neighboring residues (as shown in Tables 7–10). In all simulations (except in the AFP/ice/water simulation where the hydroxyl hydrogen of Thr-35 was replaced by the main chain amide hydrogen of Ala-36) the hydroxyl hydrogens of residues Thr-13, Thr-24, and Thr-35 hydrogen-bonded to the carbonyl oxygens of Ala-9, Ala-20, and Ala-31, respectively. Moreover, the -OH group of the Thr residues tended to point toward the N-terminal region and from visual inspection we found that the -CH_3 groups of the Thr resi-

TABLE 4 The side-chain dihedral angles and their root-mean-square fluctuations for the AFP/ice/water simulation

	χ_1	χ_2	χ_3	χ_4	χ_5	χ_6
Residue						
Asp-1	172	−155	28			
Thr-2	−109	10				
Ser-4	−42					
Asp-5	167	−132	49			
Leu-12	−69	169	−69			
Thr-13	−172	−52				
Asn-16	179	−100	79			
Lys-18	−69	−162	125	151		
Glu-22	−67	−67	−48	132		
Leu-23	−69	171	−67			
Thr-24	−170	−50				
Asn-27	172	62	−118			
Thr-35	−106	15				
Arg-37	−61	−169	−178	−171	1.5	−179
Fluctuations						
Asp-1	8	13	14			
Thr-2	40	39				
Ser-4	16					
Asp-5	10	17	17			
Leu-12	9	12	13			
Thr-13	8	8				
Asn-16	9	15	15			
Lys-18	8	47	60	84		
Glu-22	9	11	26	26		
Leu-23	10	12	13			
Thr-24	9	9				
Asn-27	9	16	16			
Thr-35	33	33				
Arg-37	11	26	12	34	13	13

dues extend out and were tilted toward the C-terminus direction. This is consistent with the geometric constraints that are required to avoid steric clashes. In the central region of the peptide in the gas phase and in the AFP/ice simulation, the carboxylate group of Glu-22 formed hydrogen bonding interactions with the ammonium group of Lys-18. Not unexpectedly, this interaction was lost in the aqueous phase and AFP/ice/water simulations due to competition between the salt bridging interaction and water. The N-terminal region in all simulations resulted in rather complicated hydrogen bonding patterns that bore some similarity to the N-terminal capping interaction described by Sicheri and Yang (1995). Finally, we note that at the C-terminal region complicated hydrogen bonding interactions arose between Thr-35–Arg-37 in all cases except in the AFP/ice/water simulation, where many of the hydrogen-bonding interactions were lost. Further details of the intrapeptide hydrogen bonding interactions among the side chain groups are detailed in the supplementary material.

For the two mutants in the gas and adsorbed phase the hydrogen bond formed by the backbone carbonyl oxygen and the backbone amide hydrogen of the fourth residue along the helix, denoted as the (i, i + 4) hydrogen bond, were found to be intact for >95% of the time except at the two ends of the helix. This is consistent with the helix content estimated based on backbone torsional angles.

The hydrogen bonds formed by any hydrogen and acceptor atom on the side chains of all the residues are retained when compared to the native peptide in the gas phase. For example, the hydroxyl group of Thr-16 in S23 (Thr-13 in the native AFP) folds back toward the N-terminal region and hydrogen-bonds to the backbone oxygen of the fourth residue (here Leu-12). Both the N- and C-terminal hydrogen bond "caps" or networks are maintained. The salt bridge between the two oppositely charged residues Lys-18 and Glu-22 were retained in both mutants.

Thr-Thr and Asx-Asx distances

An ideal α-helix has 3.6 residues per turn and traverses 5.41 Å per turn. The 11-residue repeat of the Thr residues almost completes three turns, thus, the Thr residues remain on one side of the α-helix. This repeat distance almost matches the ice lattice constant along the $\langle\bar{1}102\rangle$ direction and the spacing between the Thr hydroxyl groups are thought to be critical to the ice-binding function of this peptide (Knight et al., 1991). Here, we examine the structural details of the Thr residues for the four simulations. In addition, distances between Asp-5, Asn-16, Asn-27, and Arg-37 were also investigated since these residues are also evenly spaced along the α-helix. Furthermore, these charged and highly polar residues can potentially bind to ice quite strongly.

Table 11 lists the distances between the hydroxyl oxygens and hydrogens of two neighboring Thr residues. The root-mean-square fluctuations of the distances are also listed in Table 11. The Thr-13–Thr-24 distance of 16.4 Å in the AFP/ice phase and 16.3 Å in the AFP/ice/water phase are very close to the ice lattice constant of 16.7 Å. The distance for this pair of Thr residues also has smaller fluctuations compared to those of Thr-2–Thr-13 and Thr-24–Thr-35 when adsorbed. These latter distances fluctuate more because one of the residues is close to the N- or C-terminus of the α-helix, both of which tend to experience greater "fraying" in both adsorbed phases (see Figs. 1 and 2). Nonetheless, the average distances between the various Thr residues in the adsorbed phase only differ from the lattice spacing of the $\langle\bar{1}102\rangle$ direction by $<\pm 2$ Å. The Thr distances in the gas phase show reduced fluctuations because the hydroxyl hydrogens were hydrogen-bound to the backbone more strongly in the gas phase than in the other phases.

The distances between the Asx residues, i.e., between the carboxylate oxygens of Asp-5 and the side chain amides of Asn-16, between the side chain amides of Asn-16 and Asn-27, and between the side chain amide of Asn-27 and the side chain of Arg-37, were also estimated (see Table 11). The fluctuations in the two adsorbed phases are lower than that in the solvated phase because the carboxylate group of Asp-5 and the amide side chain of the Asn residues are hydrogen-bound to the ice surface. In the gas phase the charged side chains at the two ends of the helix form hydrogen bond "caps," hence, the Asp-5–Asn-16 and the Asn-27–Arg-37 distances fluctuate less than that between

TABLE 5 The side-chain dihedral angles and their root-mean-square fluctuations for selected residues of the S11 mutant AFP in the gas and adsorbed phases

Residue	χ_1	$\Delta_{\chi 1}$	χ_2	$\Delta_{\chi 2}$	χ_3	$\Delta_{\chi 3}$
Mutant S11 of AFP in gas phase						
Thr-2	−119 ±	29	0.5 ±	28		
Thr-13	−149 ±	41	−30 ±	42		
Asn-16	174 ±	13	159 ±	79	−21 ±	80
Thr-24	−158 ±	33	−38 ±	33		
Asn-30	171 ±	14	128 ±	81	−52 ±	81
Thr-35	−143 ±	40	−23 ±	41		
Mutant S11 of AFP on ice						
Thr-2	−96 ±	14	23 ±	14		
Thr-13	−173 ±	8	−53 ±	8		
Asn-16	158 ±	8	−122 ±	12	57 ±	12
Thr-24	−173 ±	8	−54 ±	7		
Asn-30	166 ±	14	152 ±	90	−27 ±	90
Thr-35	−70 ±	11	50 ±	11		

Asn-16 and Asn-27. The side chains in the solvated phase show the largest fluctuation since the charged chains extend into water and are more mobile. The distance between the pairs in the middle, (i.e., Asn-16–Asn-27) matches the ice lattice constant of the $\langle \bar{1}102 \rangle$ direction within 1 Å. The other distances agree with the ice lattice spacing within ±2.6 Å.

AFP-water interactions

Binding energy

In this section the details of the AFP and water (both as solvent and ice) interactions will be analyzed. The configuration energies were estimated for intra-AFP and AFP-water interactions. The intrapeptide potential energies are −1366 kcal/mol, −1170 kcal/mol, −1314 kcal/mol, and −1123 kcal/mol for the gas, aqueous, and adsorbed AFP in the gas and aqueous phases, respectively. In water and on ice, the intrapeptide energy was sacrificed to minimize the total configuration energy of the system. Thus, the intra-AFP energy becomes higher by 196 kcal/mol, 52 kcal/mol, and 244 kcal/mol for the solvated, AFP/ice, and AFP/ice/water runs, respectively. The detailed analysis of each component of the energy suggests that for the solvated phase, the intrapeptide electrostatic and 10–12 hydrogen-bonding interactions increase and van der Waals, bond, angle, and torsion energies were lowered somewhat. However, for the neat adsorbed phase the increase in the intrapeptide energy was contributed by electrostatic, 10–12 hydrogen-bonding, and torsion interactions (see the potential energy expression above). The difference in the energy change between the aqueous and neat adsorbed phases is related to the different water structures in the two cases. In the aqueous phase the water molecules were relatively mobile and the AFP structure was able to relax in order to simultaneously optimize geometric constraints (i.e., bond, angle, torsion) and water-peptide interactions. This led to a reduction in the intrapeptide electrostatic interactions and an enhancement of the peptide-water electrostatic interactions. On the other hand, the water molecules in the ice slab are confined to the crystal lattice sites and the AFP molecule needs to retain its overall shape. When both ice and water were present intrapeptide interactions were sacrificed to minimize the total configurational energy (more precisely, free energy) of the system.

TABLE 6 The side-chain dihedral angles and their root-mean-square fluctuations for selected residues of the S23 mutant AFP in the gas and adsorbed phases

Residue	χ_1	$\Delta_{\chi 1}$	χ_2	$\Delta_{\chi 2}$	χ_3	$\Delta_{\chi 3}$
Mutant S23 of AFP in gas phase						
Thr-2	−108 ±	25	11 ±	24		
Asn-13	171 ±	13	27 ±	77	−153 ±	77
Thr-16	−169 ±	9	−49 ±	8		
Thr-24	−171 ±	9	−51 ±	8		
Asn-30	171 ±	14	161 ±	89	−19 ±	89
Thr-35	−83 ±	36	38 ±	36		
Mutant S23 of AFP in gas phase						
Thr-2	−100 ±	24	19 ±	23		
Asn-13	172 ±	7	−102 ±	11	77 ±	10
Thr-16	−68 ±	8	53 ±	8		
Thr-24	−170 ±	8	−50 ±	8		
Asn-30	165 ±	20	142 ±	82	−38 ±	82
Thr-35	−86 ±	28	33 ±	27		

TABLE 7 Intra-AFP hydrogen bonds formed between the side-chain hydrogen atoms and all acceptor atoms in the gas phase

A-H(A)	D-H-A angle (°)	Probability	Acceptor	Residue	H atom	Residue
1.93	158	0.99	O	Ala-9	HOG	Thr-13
1.92	158	0.99	O	Ala-20	HOG	Thr-24
1.92	158	0.98	O	Ala-31	HOG	Thr-35
1.93	132	0.39	OD1	Asp-1	HN3	Asp-1
1.91	163	0.65	OD1	Asp-1	HN	Ala-3
1.84	150	0.61	OD1	Asp-1	HN	Ser-4
1.88	156	0.56	OD1	Asp-1	HOG	Ser-4
1.84	162	0.44	OD1	Asp-1	HN	Asp-5
1.92	137	0.70	OD2	Asp-1	HN	Thr-2
1.95	153	0.93	OD2	Asp-1	HOG	Thr-2
1.93	165	0.42	OD2	Asp-1	HN	Ala-3
2.06	156	0.43	OD2	Asp-1	HOG	Ser-4
1.82	134	0.76	OD1	Asp-5	HN2	Asp-1
1.81	135	0.10	OD1	Asp-5	HN3	Asp-1
1.83	140	0.95	OD2	Asp-5	HN	Ala-6
1.82	137	0.62	OD2	Asp-5	HN3	Asp-1
1.78	142	0.11	OD2	Asp-5	HN1	Asp-1
2.22	127	0.14	O	Lys-18	HN	Ala-21
1.77	139	0.16	OE1	Glu-22	HNZ1	Lys-18
1.77	136	0.49	OE1	Glu-22	HNZ2	Lys-18
1.75	138	0.24	OE1	Glu-22	HNZ3	Lys-18
1.77	137	0.24	OE2	Glu-22	HNZ1	Lys-18
1.76	139	0.16	OE2	Glu-22	HNZ3	Lys-18
1.77	137	0.53	OE2	Glu-22	HNZ2	Lys-18
2.08	132	0.80	OG1	Thr-35	HN	Ala-36
1.85	148	0.99	O	Ala-33	HN11	Arg-37
1.90	142	0.95	O	Ala-34	HN12	Arg-37
1.88	142	0.97	OXT	Arg-37	HNE	Arg-37
1.99	137	0.74	O	Thr-35	HN22	Arg-37
1.78	143	0.98	O	Arg-37	HN21	Arg-37
2.33	129	0.14	O	Ala-31	HN	Ala-34
2.16	131	0.17	O	Ala-32	HN	Thr-35
2.27	130	0.22	O	Thr-35	HN	Arg-37
1.81	122	0.14	O	Arg-37	HN	Arg-37
2.40	137	0.11	NH2	Arg-37	HN	Arg-37

The interaction energies between the AFP and water were −1167.4 kcal/mol and −218.7 kcal/mol for the AFP/water and AFP/ice systems, respectively. The interaction for the former was stronger due to the fact that the AFP was immersed completely in water, while it was only partially in contact with the ice surface in the latter. Furthermore, in the aqueous phase simulations the peptide partially frays at the ends, which results in more extensive hydrogen bond contacts between the water and peptide. In the AFP/ice/water simulation the AFP interacts with both ice and liquid water, and the AFP-ice and AFP-water energies were −157 kcal/mol and −905 kcal/mol, respectively. These two numbers are smaller than the corresponding values in the AFP/ice and AFP/water simulations due to the competition for the AFP between ice and water. Here, the combined AFP-ice and AFP-water interaction, −1062 kcal/mol, is, in fact, higher (i.e., more positive) than that in the AFP/water simulation. It seems that three components intra-AFP, AFP-ice, and AFP-water interactions are all sacrificed to minimize the total energy of the system, which also includes water-water, ice-ice, and ice-water interactions. Nevertheless, the AFP remained bound to the ice surface even when immersed in aqueous solution.

Solvent structure and AFP-water hydrogen bonding

The details of the AFP-water hydrogen bonding interactions were analyzed using the same criteria as adopted previously (see Intrapeptide hydrogen bond section). This analysis was carried out for all the hydrogen and acceptor atoms in the AFP and water. Similarly, the probability, the average H-acceptor distance, and donor-H-acceptor angle were calculated. The number of hydrogen bonds between each residue and water is presented in Figure 3 for the solvated and adsorbed runs in the gas phase and in aqueous solution. For the solvated phase, not unexpectedly, residues with polar and charged side chains form at least one hydrogen bond with water. For example, the charged residues Asp-1,

TABLE 8 Intra-AFP hydrogen bonds formed between the side-chain hydrogen atoms and all acceptor atoms in the aqueous phase

A-H(A)	D-H-A angle (°)	Probability	Acceptor	Residue	H atom	Residue
1.93	156	0.85	O	Ala-9	HOG	Thr-13
1.94	156	0.80	O	Ala-20	HOG	Thr-24
1.92	156	0.53	O	Ala-31	HOG	Thr-35
2.09	133	0.39	O	Asp-1	HN	Ala-3
2.15	141	0.44	O	Thr-2	HN	Asp-5
2.18	131	0.15	O	Ala-3	HN	Ala-6
2.20	127	0.13	O	Lys-18	HN	Ala-21
2.24	130	0.12	O	Ala-20	HN	Leu-23
2.08	140	0.19	O	Ala-21	HOG	Thr-24
2.27	127	0.11	O	Leu-23	HN	Ala-26
2.21	133	0.12	O	Ala-31	HN	Ala-34
2.01	156	0.30	O	Ala-31	HN	Ala-36
2.22	129	0.11	O	Ala-32	HN	Thr-35
2.23	135	0.11	O	Ala-33	HN	Ala-36
1.98	142	0.19	O	Ala-33	HN21	Arg-37
1.89	152	0.37	O	Ala-33	HNE	Arg-37
2.20	156	0.16	O	Ala-34	HN	Arg-37
2.03	142	0.72	O	Thr-35	HN	Arg-37

Asp-5, Glu-22, and Arg-37 each form more than eight hydrogen bonds with water, while Lys-18, Asn-16, and Asn-27 hydrogen bond to almost four water molecules. The side chains of Thr-13, Thr-24, and Thr-35 hydrogen bond to one or two water molecules, while most backbone carbonyl oxygen atoms form very short-lived hydrogen bonds with water. The backbone amide hydrogens of Asp-1, Thr-2, Ala-3, and Ser-4 also appear to form transient hydrogen bonds with water.

For the adsorbed phases without and with water, due to the limited contact with ice, the numbers of hydrogen bonds are smaller than in the solvated phase. However, it appears that Asp-5, Asn-16, Asn-27, and Arg-37 form more hydrogen bonds with the ice surface than do the Thr residues (numbers 2, 13, 24, 35).

For the adsorbed phase in aqueous solution the AFP stays in contact with the ice surface. Here, we separate the hydrogen bonds into two groups: AFP-ice and AFP-water. The number of hydrogen bonds for each group is shown in Fig. 3 together with the other two runs. The number of hydrogen bonds for each residue with the ice surface is very similar to that in the neat adsorbed phase and the AFP-water hydrogen bond pattern is similar to that observed in the solvated phase. We find that Asn-16 and Asn-27 form fewer hydrogen bonds with water and are bound more strongly to ice and this is also true for the Thr residues. Asp-1 and Asp-5, on the other hand, interact strongly with both water and ice molecules. The C-terminal end extends somewhat more into water and is frayed more than in the neat solvated simulation, which results in only one hydrogen bond being formed between Arg-37 and ice. Consequently, the six C-terminal residues form more hydrogen bonds with water when compared to the neat solvated phase.

We examined the probability, H-acceptor distance, and donor-H-acceptor angle for the AFP-water hydrogen bonds that are present for >10% of the time in the aqueous phase simulation. It is clear that most hydrogen bonds are formed by the atoms on the side chains of the AFP for the solvated phase. Almost all backbone carbonyl oxygens hydrogen-bond weakly with water for some short period of time. All three ammonium hydrogens of Lys-18 and the two carboxyl oxygens of Glu-22 hydrogen-bond strongly to water molecules. Thus, these interactions eliminate the salt bridge observed in the gas phase simulation.

For the AFP on ice only the Thr, Asx, and Arg residues hydrogen bond to the ice (see Table 12). Some atoms may form more than one hydrogen bond with the ice surface, thus the probabilities or the average number of hydrogen bonds are >1.0. Lys-18 and Glu-22 stay away from the surface, and form a salt bridge in the gas phase region beyond the ice slab. For the Thr residues the hydroxyl oxygens interact with the surface while the hydroxyl hydrogens form intrapeptide hydrogen bonds. The side chain amide oxygen, nitrogen, and one of the hydrogen atoms on the Asn side chains (Asn-16 and Asn-27) are solely responsible for the hydrogen bonding with the surface. The hydrogen-bonding pattern observed here strongly suggests that Asx residues are very important in the ice-binding function of the AFPs. Asp-5, Asn-16, and Asn-27 are also arranged in 11 residue repeats similar to the Thr residues. Thus, it seems that the Thr and Asx residues bind to the surface cooperatively.

Similar to the AFP/ice system, only the Asx, Thr, and Arg residues bind to the ice surface in the AFP/ice/water system (see Table 13). Overall, the number of hydrogen bonds for most ice-binding residues are slightly lower than that in the

TABLE 9 Intra-AFP hydrogen bonds formed between the side-chain hydrogen atoms and all acceptor atoms in the AFP/ice simulation

A-H(A)	D-H-A angle (°)	Probability	Acceptor	Residue	H atom	Residue
1.92	160	0.99	O	Ala-9	HOG	Thr-13
1.97	160	0.98	O	Ala-20	HOG	Thr-24
2.04	144	0.20	O	Ala-31	HOG	Thr-35
2.27	127	0.10	O	Ala-8	HN	Ala-11
2.26	127	0.10	O	Ala-21	HN	Thr-24
2.11	130	0.20	OD1	Asp-1	HN	Thr-2
2.01	153	0.38	OD1	Asp-1	HOG	Thr-2
1.84	163	1.00	OD1	Asp-1	HN	Ala-3
1.93	156	0.75	OD1	Asp-1	HN	Ser-4
2.02	160	0.64	OD1	Asp-1	HOG	Ser-4
1.86	135	0.97	OD2	Asp-1	HN3	Asp-1
1.98	142	0.33	OD2	Asp-1	HN	Ser-4
1.96	150	0.31	OD2	Asp-1	HOG	Ser-4
1.83	163	0.73	OD2	Asp-1	HN	Asp-5
1.78	140	0.49	OD1	Asp-5	HN1	Asp-1
2.10	126	0.14	OD1	Asp-5	HN	Asp-5
2.17	128	0.16	OD1	Asp-5	HN	Ala-6
1.77	138	0.95	OE1	Glu-22	HNZ1	Lys-18
1.77	135	0.89	OE2	Glu-22	HNZ3	Lys-18
2.20	128	0.22	O	Lys-18	HN	Ala-21
2.21	129	0.18	OG1	Thr-35	HN	Ala-36
1.98	154	0.86	O	Ala-31	HN	Ala-36
1.99	149	0.27	O	Ala-33	HN12	Arg-37
1.86	146	0.75	O	Ala-34	HN12	Arg-37
1.86	144	0.21	O	Ala-32	HN22	Arg-37
2.04	130	0.18	O	Ala-32	HN21	Arg-37
1.90	156	0.84	O	Ala-33	HN22	Arg-37
2.05	134	0.74	O	Ala-36	HN21	Arg-37
1.99	136	0.87	O	Ala-36	HNE	Arg-37

neat adsorbed phase. For example, Arg-37 only forms one hydrogen bond with the ice surface and Thr-2 no longer forms long-lived hydrogen bonds with the ice surface. However, Asp-1, Asn-27, and Thr-35 form stronger interactions with the ice surface. Lys-18 and Glu-22 hydrogen-bond exclusively to solvent as in the neat solvated phase, which again results in the loss of the salt-bridge interaction. The carbonyl oxygens of the Ala residues form hydrogen bonds with solvent molecules with a probability ranging from 0.1 to 1. (This is also observed in the AFP/water simulation.) In

TABLE 10 Intra-AFP hydrogen bonds formed between the side-chain hydrogen atoms and all acceptor atoms in the AFP/ice/water simulation

A-H(A)	D-H-A angle (°)	Probability	Acceptor	Residue	H atom	Residue
1.94	156	0.98	O	Ala-9	HO	Thr-13
1.91	156	0.87	O	Ala-20	HOG	Thr-24
2.02	150	0.87	O	Ala-31	HN	Ala-36
2.22	128	0.14	O	Ala-8	HN	Ala-11
2.16	129	0.19	O	Ala-26	HN	Ala-29
1.96	139	0.71	O	Asp-1	HN	Ala-3
2.13	148	0.82	O	Asp-1	HN	Ala-6
2.10	163	0.17	OD2	Asp-1	HN	Ala-3
2.22	129	0.10	O	Ser-4	HN	Ala-7
2.27	129	0.14	O	Asp-5	HN	Ala-8
1.76	163	0.83	OD1	Asp-5	HN2	Asp-1
2.25	129	0.14	O	Lys-18	HN	Ala-21
2.21	129	0.12	O	Ala-19	HN	Glu-22
2.24	137	0.10	O	Thr-24	HN	Asn-27

TABLE 11 The Thr-Thr and Asx-Asx distances and their root-mean-square fluctuations for the four simulations

		Gas Phase		Aqueous Phase		AFP/Ice		AFP/Ice/Water	
Thr-Thr Distances									
O atom									
Thr-2–Thr-13		18.7	0.5	16.2	1.0	17.2	1.0	14.9	0.7
Thr-13–Thr-24		16.5	0.4	16.6	0.5	16.4	0.3	16.3	0.3
Thr-24–Thr-35		16.2	0.4	16.6	1.2	15.4	0.5	18.5	1.0
H atom									
Thr-2–Thr-13		17.4	0.6	15.9	0.9	16.2	1.0	15.0	0.8
Thr-13–Thr-24		16.5	0.4	16.8	0.5	16.4	0.3	16.4	0.5
Thr-24–Thr-35		16.2	0.4	16.6	1.4	15.6	0.6	18.1	1.0
Asx-Asx Distances									
Asp-5 OD1	Asn-16 OD1	19.2	0.7	17.1	0.8	17.6	0.3	17.4	0.6
Asp-5 OD1	Asn-16 ND1	19.4	0.8	17.1	1.0	19.2	0.3	18.0	0.6
Asp-5 OD2	Asn-16 OD1	18.7	0.7	16.8	0.9	16.5	0.3	16.2	0.4
Asp-5 OD2	Asn-16 ND1	18.9	0.7	16.9	1.1	18.0	0.3	16.6	0.5
Asn-16 OD1	Asn-27 OD1	16.4	0.9	16.8	1.0	17.7	0.5	16.5	0.4
Asn-16 OD1	Asn-27 ND1	16.4	0.9	16.7	0.9	17.2	0.4	17.1	0.5
Asn-16 ND1	Asn-27 OD1	16.2	0.9	16.8	1.1	16.1	0.5	16.1	0.4
Asn-16 ND1	Asn-27 ND1	16.2	1.0	16.8	1.0	15.8	0.3	17.0	0.4
Asn-27 OD1	Arg-37 O	17.4	0.8	17.7	1.5	13.8	1.3	13.6	0.9
Asn-27 OD1	Arg-37 OXT	18.1	0.7	17.1	1.4	14.5	1.1	13.5	1.3
Asn-27 ND1	Arg-37 O	17.1	0.7	17.4	1.9	13.4	1.2	13.6	0.9
Asn-27 ND1	Arg-37 OXT	17.8	0.7	16.9	1.7	14.2	1.0	13.2	1.3
Asx-Thr Distances									
Thr-2 OG1	Asp-5 OD1	8.1	0.3	6.3	0.8	7.6	0.3	8.0	0.8
Thr-2 OG1	Asp-5 OD2	7.5	0.3	6.9	0.6	9.5	0.5	9.8	0.7
Thr-13 OG1	Asn-16 OD1	7.5	0.7	7.7	0.9	6.1	0.3	7.2	0.4
Thr-13 OG1	Asn-16 OD2	7.5	0.8	7.7	0.8	8.0	0.3	8.3	0.4
Thr-24 OG1	Asn-27 OD1	7.6	0.7	8.2	0.7	8.1	0.4	8.2	0.4
Thr-24 OG1	Asn-27 OD2	7.3	0.8	8.2	0.9	6.8	0.3	8.0	0.4
Thr-35 OG1	Arg-37 O	7.8	0.2	9.9	0.5	7.9	1.0	8.7	0.5
Thr-35 OG1	Arg-37 OXT	9.2	0.2	8.8	0.6	8.6	1.0	9.7	0.5

particular, those for Ala-9, Ala-20, and Ala-31 have probabilities <0.15 since those oxygen atoms form very stable hydrogen bonds with hydroxyl hydrogens of Thr-13, Thr-24, and Thr-35, respectively. In both the AFP/water and AFP/ice/water systems, Ser-4 forms 3–4 hydrogen bonds with water, among those two are due to the side chain -OH group.

Ice-binding pattern

In what follows we will examine the ice-binding pattern in the AFP/ice system in detail. We note that the pattern observed in the AFP/ice/water system is very similar to the AFP/ice system, so we do not discuss the former system in detail. The snapshot of the AFP adsorbed on ice given in Fig. 4 clearly shows that the helix lies along the $\langle\bar{1}102\rangle$ direction. Fig. 5 is a snapshot viewed along the $\langle 010\rangle$ direction, which intersects the $\langle\bar{1}102\rangle$ direction by 66°. Note that in Figs. 4 and 5 the $\langle 010\rangle$ direction is not perpendicular to the helix axis. The binding atoms can be divided into four ice-binding groups: Asp-1/Thr-2/Asp-5, Thr-13/Asn-16, Thr-24/Asn-27, and Thr-35/Arg-37. The Thr and Asx in the first three groups are three residues apart, which is not enough to move through a complete α-helical turn. In the ideal α-helix case, they are 60° apart about the helix axis. Both residues face the ice surface with their respective side chains in contact with the ice surface.

First we examined the two central ice-binding groups (Thr-13/Asn-16 and Thr-24/Asn-27) of the α-helix. The two groups in the interior of the helix are exactly one lattice constant apart along the ice $\langle\bar{1}102\rangle$ direction. The distance between the backbone atoms, Cα, N, and O of Thr and Asn residues within the same group is ~4.9 Å. The vector connecting the corresponding backbone atoms of the two residues intersects the $\langle\bar{1}102\rangle$ direction by 20–30°. The distance between the side chain functional groups of the two residues in each pair ranges from 6.0 to 10.0 Å (see Tables 9 and 10, Thr-Asx Distances section). The vectors connecting the ice-binding region on the two residues also intersects the $\langle\bar{1}102\rangle$ direction by roughly the same angle as the backbone atoms. Thus, the binding groups do not align parallel to the $\langle 010\rangle$ direction, which intersects the $\langle\bar{1}102\rangle$ axis by 66°. This finding does not support the proposed alignment direction based on x-ray experiments (Sicheri and Yang, 1995). The snapshot in Fig. 6 shows the alignment of water bound Thr-Asn atoms relative to the ice lattice. For the AFP/ice system, 21 bound water molecules were identified from the hydrogen bond list. Fig. 7 shows the space-

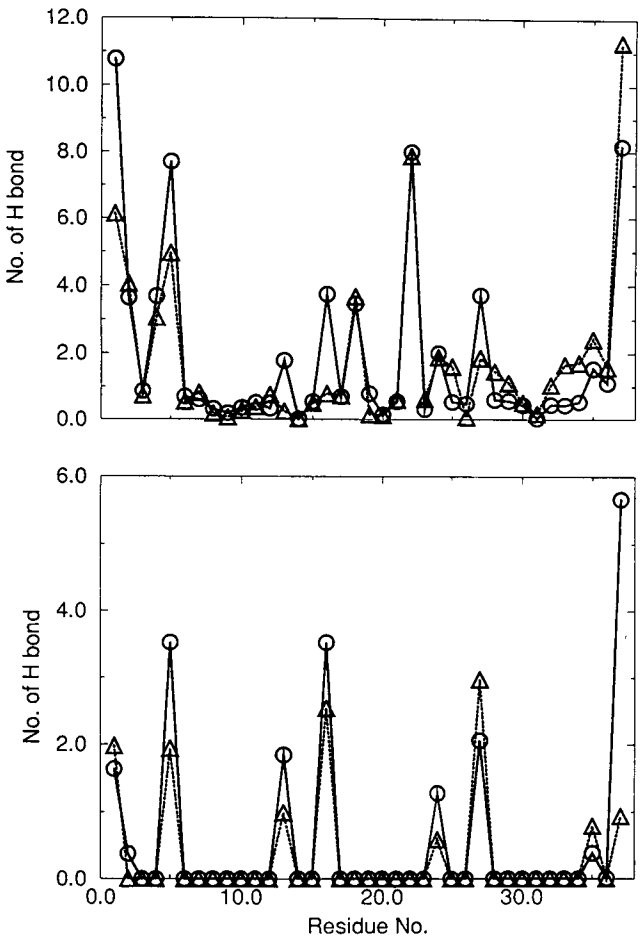

FIGURE 3 Number of hydrogen bonds formed by each residue of the AFP with water molecules. The top panel is for the AFP-water hydrogen bonds in solvated (*circles*) and in the AFP/ice/water (*triangles*) phases. The bottom panel is for AFP-ice hydrogen bonds in the AFP/ice (*circles*) and AFP/ice/water (*triangles*) phases.

TABLE 12 AFP-ice hydrogen bonding parameters for the AFP/ice simulation

A-H Distance (Å)	No. of H Bonds	AFP Atom	Residue
2.27	0.12	HN1	Asp-1
1.82	1.04	HN2	Asp-1
2.16	0.48	O	Asp-1
2.12	0.17	HOG	Thr-2
2.17	0.19	OG1	Thr-2
1.94	0.61	OD1	Asp-5
1.92	2.80	OD2	Asp-5
2.29	0.11	O	Asp-5
2.05	1.85	OG1	Thr-13
2.05	0.94	HND2	Asn-16
2.00	1.94	OD1	Asn-16
2.16	0.65	ND2	Asn-16
2.13	1.28	OG1	Thr-24
1.95	0.99	HND2	Asn-27
2.00	0.83	OD1	Asn-27
2.26	0.24	ND2	Asn-27
2.02	0.28	O	Thr-35
2.22	0.63	HN	Arg-37
1.97	2.66	O	Arg-37
1.99	2.36	OXT	Arg-37

filling snapshot of the AFP with bound water molecules. All 21 water molecules are located in the top three lattice planes of the ice surface. The distance between the first and second layer and the second and third layers of ice are 0.5 Å and 0.3 Å, respectively. The arrangement of the five bound water molecules to the two groups in the middle of the helix show a very similar binding pattern (Fig. 6). The Thr residues hydrogen-bond to two water molecules in the top layer. These two water molecules line up along ⟨010⟩ direction and are 4.5 Å apart. The hydroxyl oxygen of the Thr residue sits above and between these water molecules, and forms hydrogen bonds with three or four water hydrogen atoms (Fig. 8). The three water molecules bound to each Asn residue form a triangle, although one is located in the second layer and two in the third layer. The latter two water molecules align along the ⟨010⟩ direction and are 4.5 Å apart. The binding group of Asn (i.e., the side chain amide nitrogen, oxygen, and one of the hydrogen atoms) sits above the water triangle and orients in such a way to optimize the number of hydrogen bonds formed with the corresponding water molecules (Fig. 8).

The side-view snapshot (Fig. 5) shows that the surface has ridge/step/valley topology along the ⟨$\bar{1}$102⟩ direction. The ridge and valley align along the ⟨010⟩ direction. Thr-13 and Thr-24 hydrogen-bond to the water molecules on the ridge (top layer of the ice lattice) while Asn-16 and Asn-27 hydrogen-bond to the water in the step (second and third layer of ice lattice). Examination of the average vertical distance of binding atoms to the ice surface can give some information on how flat or corrugated the surface is. The average distance of the binding atom to the corresponding binding plane ranges from 1.85 to 2.2 Å. The maximum difference of the vertical coordinates of the four binding atoms of Thr-13/Asn-16 and Thr-24/Asn-27 is 1.25 Å. The hydroxyl oxygens of the Thr residues are furthest away from the ice surface since these residues bind to the top water layer, while the amide hydrogens of the Asn residues extend down the most. One can also compare the overall topology of the AFP, i.e., the surface formed by all the atoms facing the ice. The largest distance to the surface is no more than 2 Å.

The binding group at the N-terminal region of the helix, Asp-1/Thr-2/Asp-5, also shows a similar binding pattern. Similar to Asn-16 and Asn-27 the two carboxyl oxygens of Asp-5 bind to three water molecules that are located exactly one lattice constant away from the neighboring binding group. Due to the uncoiling of the helix at the N-terminal region Thr-2 binds to two water molecules located on the step. Asp-1 folds back and binds to one water on the ridge.

TABLE 13 AFP-ice hydrogen bonding parameters for the AFP/ice/water simulation

A-H Distance (Å)	No. of H Bonds	AFP Atom	Residue
1.92	0.99	HN1	Asp-1
1.88	0.96	OD1	Asp-1
1.90	0.94	OD1	Asp-5
1.83	1.00	OD2	Asp-5
1.96	0.99	OG1	Thr-13
2.18	0.16	HND1	Asn-16
2.03	0.93	HND2	Asn-16
2.07	1.33	OD1	Asn-16
2.26	0.12	ND2	Asn-16
1.97	0.56	OG1	Thr-24
2.13	1.12	HND2	Asn-27
2.05	1.68	OD1	Asn-27
2.28	0.19	ND2	Asn-27
2.02	0.42	HOG	Thr-35
2.07	0.17	OG1	Thr-35
2.01	0.20	O	Thr-35
1.88	0.91	O	Arg-37

At the C-terminal region, Arg-37 forms five to six hydrogen bonds with five water molecules. Three of the Arg-bound water molecules form a triangle similar to the other binding groups; however, the triangle was shifted one lattice spacing along the ⟨010⟩ direction due to the slight bending of the helix at the C-terminal end. The carbonyl oxygen of Thr-35 forms a short lived hydrogen bond with one water molecule on the ridge, which is exactly one lattice constant away from one of the water molecules bound to Thr-24.

The most striking feature was the observation that Asp-5, Asn-16, Asn-27, and Arg-37 each hydrogen-bond to three water molecules in the step and the Thr residues hydrogen bond to two water molecules in the ridge. The four groups of bound water molecules align along the $\langle \bar{1}102 \rangle$ direction and are also one lattice constant apart. The arrangement of water molecules in each group is the same except for some slight adjustment due to the uncoiling of the helix at the two ends.

In the AFP/ice/water system the Asx, Thr, and Arg residues stay in contact with ice as discussed above. These residues were solely responsible for ice binding as was the case in the AFP/ice simulation discussed in detail above. However, we find that the hydroxyl oxygen of Thr-13 and Thr-24 interacts with only one water molecule on the top layer of the ice lattice as opposed to two in the AFP/ice system. In this case the -OH group sits right above an ice molecule on the ridge, thereby shifting by half a lattice spacing along the ⟨010⟩ direction relative to that observed in the AFP/ice simulation. The side chains of Asn-16 and Asn-27 hydrogen-bonded to three water molecules in the step region as was observed in the AFP/ice system. However, the center of the three Asn bound ice water molecules shift roughly by the same amount as that for the hydroxyl group of Thr. Here one of the three water molecules is in the third ice layer and two are located in the second ice layer.

Visual inspection of the trajectories show that the two mutants align along the $\langle \bar{1}102 \rangle$ direction of the ice lattice. The Lys-18/Glu-22 salt bridge stays away from the surface. Asn, Asp, Arg, and Thr residues stay on one side of the helix facing the ice surface. However, some of these residues are not in close contact with the ice surface, as will be described below. Again, all the possible hydrogen bonds formed between the peptide and ice were examined. Those hydrogen bonds with >1% probability are presented in Tables 14 and 15 (see Table 12 for the native AFP). The hydrogen bond pattern in both the N- and C-terminal regions did not change significantly except for slight variations in the calculated probability. The three hydrogen atoms of the N-terminal ammonium group are equivalent; therefore, hydrogen bonds formed by these three protons would be equivalent over very long simulation time scales. Thr-2 showed a weak ice-binding capability in the native peptide and its binding ability was further reduced in the mutants. We believe that this change is likely due to thermal fluctuations rather than some intrinsic property of the mutants.

Significant changes in ice-binding properties were observed in the mutated regions. For example, Asn-30 in S11 forms a hydrogen bond with the ice surface with only a 0.2 probability, while in the S23 mutant the probability is only 0.001 (data not shown). For S23, due to the interchange of Thr-13 and Asn-16, Thr-16 only has a hydrogen bonding probability of 0.2 while in the native and S11 mutant the probability is on the order of 1.7–1.8. The number of hydrogen bonds formed between each residue and the ice surface are graphically summarized in Fig. 9. The Asp-1/Thr-2/Asp-5 and the Thr-35/Arg-37 regions essentially have the same number of hydrogen bonds as in the native peptide. On the other hand, Asn-30 in S11 and S23 (Asn-27 in the native protein) and Thr-16 in S23 (Thr-13 in the native peptide) have essentially lost all of their hydrogen-bonding contacts. If the number of hydrogen bonds for each of the four binding groups is plotted as a function of activity (as in Fig. 10), one can see that the decrease in the number of hydrogen bonds for the two groups in the interior of the mutants is directly related to the reduction of the antifreeze activity. The estimated binding energy is also plotted as a function of activity (see Fig. 10). This figure reveals the strong correlation between the binding energy, number of hydrogen bonds and activity. The greater the number of hydrogen bonds, the stronger the binding and the greater the activity. Interestingly, the configurational energy (not shown here) of the ice slab decreases (i.e., becomes more positive) with the increase in the activity of the peptide. This is because as the hydrogen bonding between the ice and peptide becomes more favorable, this leads to a disruption in the optimal hydrogen bonding between neighboring water molecules in the ice slab. We have found that the

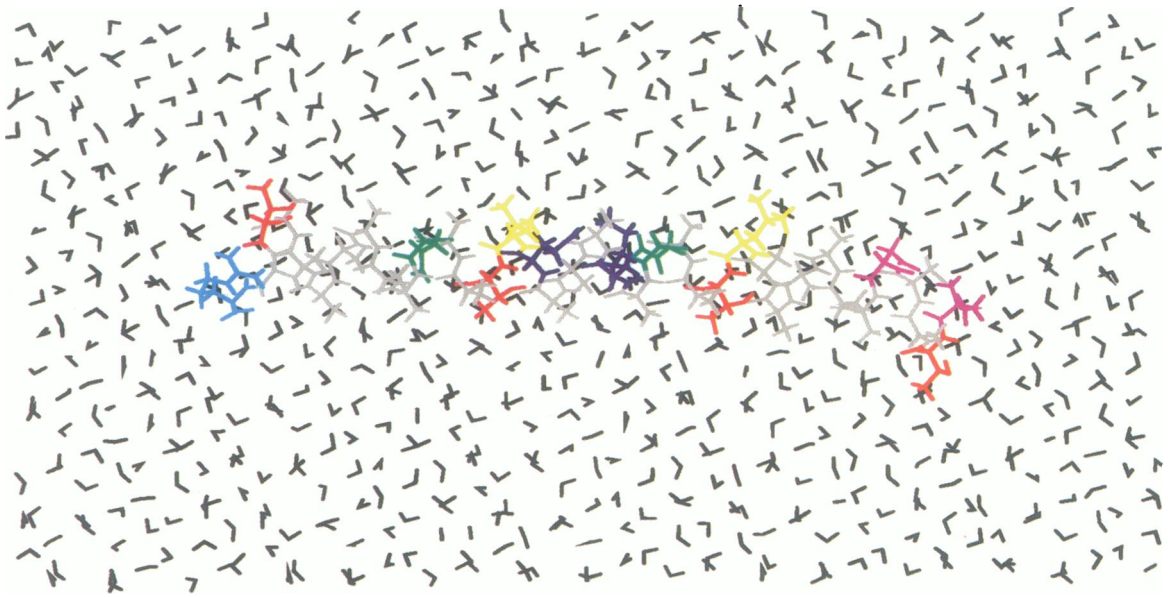

FIGURE 4 The top view of a snapshot of the AFP on the ice $(20\bar{2}1)$ surface. The residues Thr, Asp, Asn, Arg, Leu, Lys, and Glu are red, purple, green, cyan, yellow, blue, and blue, respectively. Water molecules are in black. The N-terminus starts at the right and the C-terminus is at the left of the figure. The view given intends to illustrate that the AFP aligns along the ice $\langle\bar{1}102\rangle$ direction (the x axis in the figure). The surface ridge/step/valley topology (see fig. 5 for a side view of this topology) aligns along the $\langle 010\rangle$ direction which intersects the $\langle\bar{1}102\rangle$ direction by 66°. Note that the Thr and Asx residues are evenly spaced along the helix and along the surface topology.

peptide-ice interactions include van der Waals and electrostatic interactions.

It is also known that the strength of a hydrogen bond ranges from 2 to 10 kcal/mol (Creighton, 1993). Thus, if we assume that the hydrogen bond strength is 10 kcal/mol it is clear that hydrogen bonding interactions can explain the ice binding pattern (compare the top and bottom panel in Fig. 10). On the other hand, if we use the lower value it is clear that other effects like hydrophobic interactions can play a role in governing ice binding, since this lower estimate for the strength of a hydrogen bond cannot explain the entire difference in the computed binding energy between the ice surface and the peptide (i.e., U_{bind}). Recent estimates of hydrogen bond strengths by Myers and Pace indicate that an intramolecular hydrogen bond is worth 1–2 kcal/mol in stabilizing globular proteins (Myers and Pace, 1996). Thus, in order to explain our observations we conclude that concomitant with the specific hydrogen bonding interactions being altered in the mutants, other hydrogen bonds remote from the mutation sites must also be weakened as well as favorable van der Waals present between the peptide and the surface.

In order to further understand, at the molecular level, what causes the reduction in the number of hydrogen bonds in the mutants, we examined closely the complementarity of the two Thr/Asn ice-binding groups to the ice surface. In S11 the ice-binding pattern of Thr-13/Asn-16 is relatively unaffected; however, the Thr-24/Asn-30 (Thr-24/Asn-27 in the native protein) group exhibits an altered ice-binding pattern. Specifically, Thr-24 remains bound to the water molecules on the ridge of the ice surface, while, as shown above, Asn-30 binds only very weakly with the ice surface. Since the two polar residues are three residues further apart, Asn-30 is located close to the valley of the ice surface

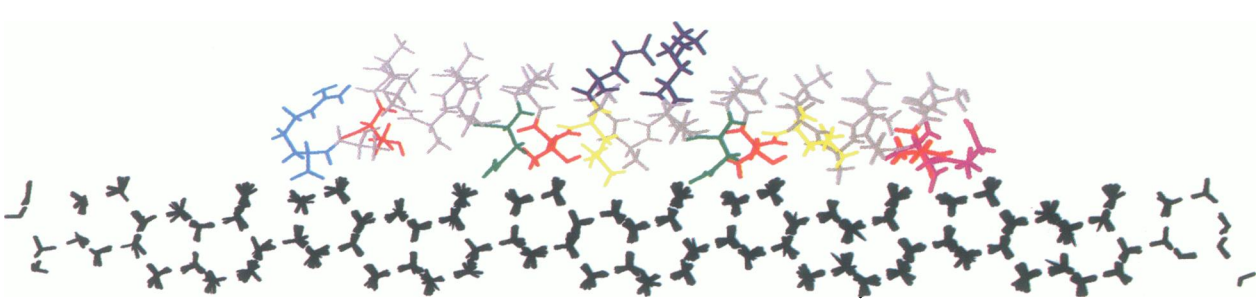

FIGURE 5 A snapshot of the AFP on the ice surface viewed along $\langle 010\rangle$ direction. The color code and sequence alignment are the same as in Fig. 4. This view shows the surface ridge/step/valley (going from right to left) topology and the AFP binding surface. The Thr residues sit above the ridge and the Asn residues sit on the step. The side chains of Ala-9, Leu-12, Ala-20, and Leu-23 point into the valleys.

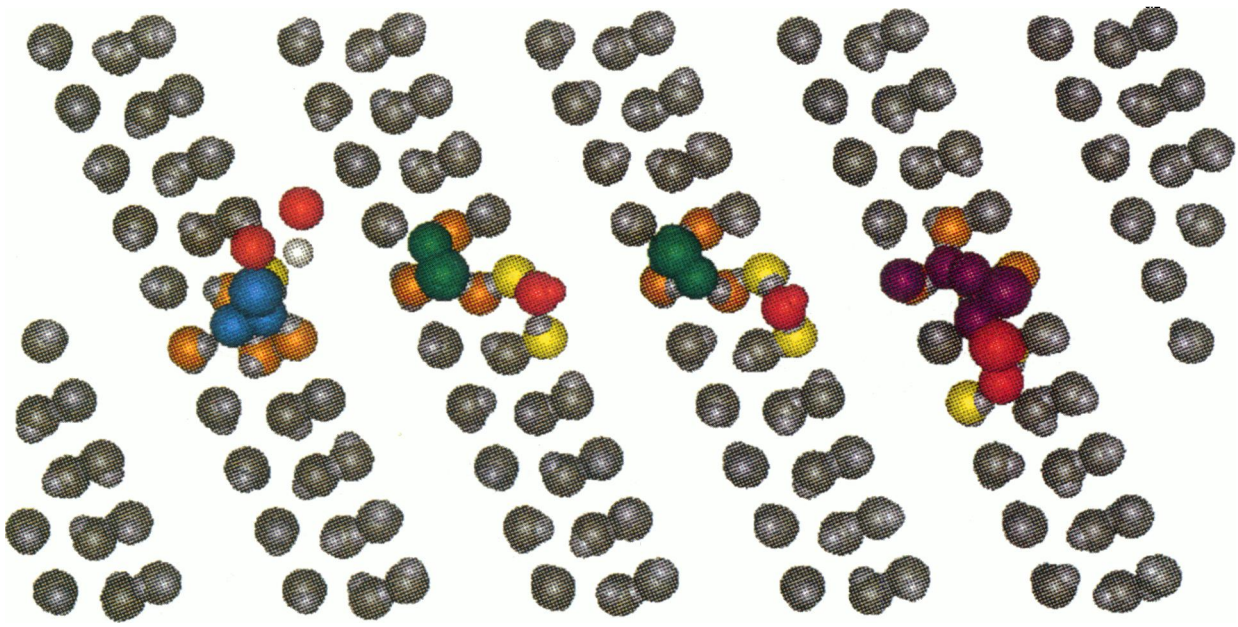

FIGURE 6 The alignment of the binding groups relative to the ice surface. The binding atoms of residues Thr, Asp, Asn, and Arg are in red, purple, green and cyan, respectively. Here, the Asn-Thr ice binding motif intercepts the $\langle\bar{1}102\rangle$ direction by 20° to 30°, which is not parallel to the $\langle 010\rangle$ direction. The location of bound water on the ice surface shows that each group is separated by one lattice spacing along the $\langle\bar{1}102\rangle$ direction. Those bound to Thr residues (water oxygens in yellow) lie along the ridge ($\langle 010\rangle$ direction) and are 4.5227 Å apart. The water molecules bound to the Asn, Asp, and Arg side chains have orange oxygen atoms.

instead of on the steps of the surface, as seen in the native peptide. Clearly, the side chain of Asn-30 is not long enough to reach the water molecules in the valley nor was it able to form stable hydrogen bonds with ice molecules on the step.

For S23 the interchange of Thr-13 and Asn-16 did not destroy the ice-binding ability completely. Thr-16 is now located above the step region of the ice surface and does not hydrogen-bond to any surface water molecules. However, the side chain of Asn-13 was able to bind to the ice molecules in the step region in order to maximize the number of hydrogen bonds. Since the ridge region only affords the ability to hydrogen bond with one row of water molecules effectively, Asn-13 moves into the step region where it can form hydrogen bonds with two rows of water molecules. This allows the Asn side chain to form as many hydrogen bonds as possible with all of its hydrogen-bonding-capable atoms. This results in hydrogen bonds with three water molecules that are just one lattice constant away from those bound by the native peptide. This places both Thr-16 and Asn-13 in the step region of the ice surface, with the result being the alignment of these two residues parallel with the $\langle 010\rangle$ direction (in the native peptide these two residues intercept the $\langle 010\rangle$ direction by 20–30°).

Overall, it appears that the Thr-Asn distance, and consequently, the binding surface formed by these two residues,

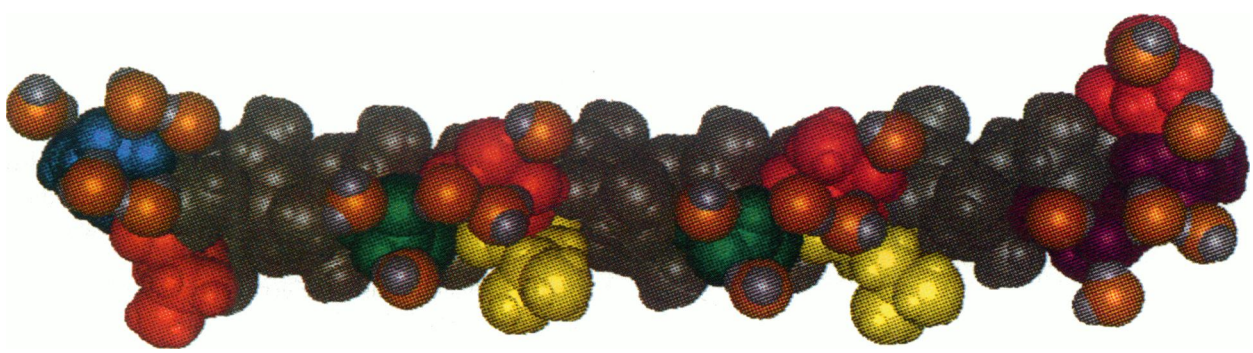

FIGURE 7 A snapshot of the AFP with 21 water molecules on the ice surfaces. The color code is the same as in Fig. 4 except the water oxygen atoms are in orange. These water molecules form long-lived hydrogen bonds with the AFP. The picture illustrates the location of these water molecules on the AFP surface. The Thr residues (*red*) each bind to two water molecules and the Asx residues (*purple* and *green*) bind to three water molecules.

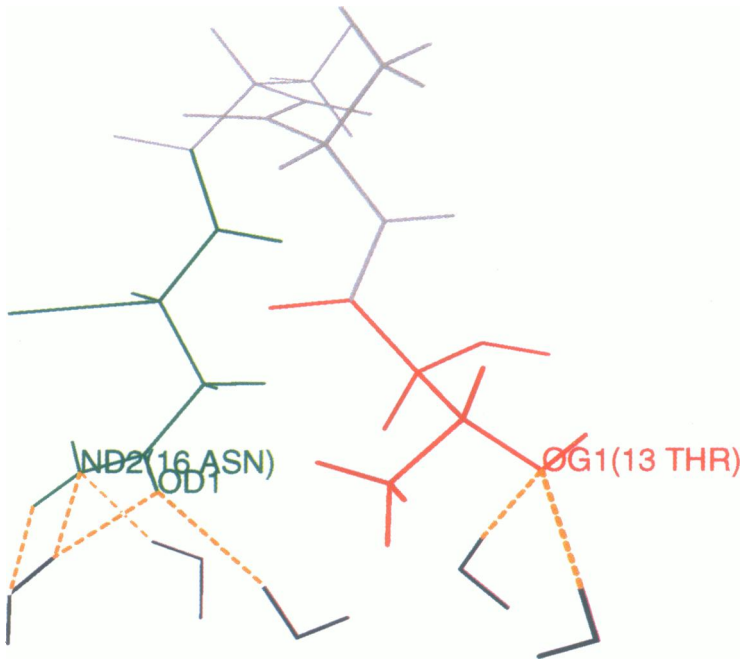

FIGURE 8 A snapshot of residues Thr-13 to Asn-16 of the AFP with five bound ice water molecules to show the hydrogen bonding pattern. The color code is the same as in Fig. 4. That of residues Thr-24 to Asn-27 of the AFP with five bound ice water molecules show a similar hydrogen bonding pattern.

is crucial to effective ice-binding. When they are further apart, as is the case in the two mutants, the binding residues lose their "precise" complementarity with the ice surface topology and, therefore, are unable to bind the ice surface effectively.

TABLE 14 Mutant S11-ice hydrogen bonding parameters

A-H distance (Å)	Probability	AFP Atom	Residue
1.90	0.28	HN1	Asp-1
1.88	0.83	HN2	Asp-1
2.16	0.45	HN3	Asp-1
2.25	0.04	O	Asp-1
1.95	1.79	OD1	Asp-5
1.86	2.00	OD2	Asp-5
2.32	0.05	O	Asp-5
2.07	1.75	OG1	Thr-13
2.04	0.03	HOG	Thr-13
1.99	1.90	OD1	Asn-16
2.14	0.72	ND2	Asn-16
2.04	0.96	HND2	Asn-16
2.14	1.11	OG1	Thr-24
2.04	0.20	OD1	Asn-30
2.22	0.03	HND2	Asn-30
2.20	0.61	OG1	Thr-35
1.98	0.91	HN	Ala-36
2.25	0.81	HN	Arg-37
1.89	2.08	O	Arg-37
1.92	1.56	OXT	Arg-37

van der Waals interaction

In addition to the polar side chains, other hydrophobic side chains also seem to play important roles in ice binding. Here, we examine the role of van der Waals interactions in AFP/ice binding. Visual inspection of the trajectories showed that the methyl groups of the Thr residues also point toward the surface to possibly maximize favorable van der Waals interactions, thus enhancing ice binding. The side chains of the two Leu residues fit into valleys on the surface, which also presumably enhances the ice binding by maximizing favorable van der Waals interactions. Two Ala residues, Ala-9 and Ala-20, which are almost three turns apart in the α-helix, are also in close contact with the surface (see Fig. 11). Their side chain -CH_3 groups point into the valleys on the surface. The methyl groups of these two Ala residues are almost in the same plane as that formed by the ice binding atoms of the charged and polar residues.

In the hydrophobic effect a water "clathrate" is formed around the hydrophobic residues, i.e., the water molecules next to the hydrophobic groups form hydrogen bonds with other neighboring water molecules, thereby sacrificing their configurational entropy (Swaminathan et al., 1978; Rossky and Karplus, 1979; Teeter, 1984). We compared the water radial distribution function g(r) in the solvated and adsorbed phases around the CH_3 groups and we calculated the average distance between CH_3 groups and the surrounding water molecules.

In the solvated phase, the g(r) between carbon atoms and water oxygen (OW) and hydrogen (HW) atoms for all the CH_3 groups show, not unexpectedly, similar features (see Fig. 12 *a* for an example). In addition, the first peak in $g_{c\text{-}ow}(r)$ and $g_{c\text{-}hw}(r)$ appears at the same position (r = 3.8 Å) even though the $g_{c\text{-}hw}(r)$ peak is typically broader. This

TABLE 15 Mutant S23-ice hydrogen bonding parameters

A-H Distance (Å)	Probability	AFP Atom	Residue
1.99	0.34	HN1	Asp-1
1.88	0.31	HN2	Asp-1
1.82	0.58	HN3	Asp-1
2.17	0.27	O	Asp-1
2.14	0.02	HOG	Thr-2
2.26	0.01	O	Thr-2
1.99	0.76	OD1	Asp-5
1.89	2.69	OD2	Asp-5
2.14	0.64	O	Asp-5
2.40	0.03	N	Asn-13
2.37	0.04	OD1	Asn-13
2.10	0.80	ND2	Asn-13
1.96	0.99	HND1	Asn-13
2.02	0.97	HND2	Asn-13
2.29	0.18	OG1	Thr-16
2.08	0.02	HOG	Thr-16
2.32	0.04	O	Thr-16
2.10	1.52	OG1	Thr-24
2.07	0.04	HOG	Thr-24
2.29	0.04	HOG	Thr-35
2.11	0.52	O	Thr-35
2.21	0.27	HN	Arg-37
2.00	2.34	O	Arg-37
2.01	3.00	OXT	Arg-37
2.37	0.01	N	Ala-6
2.28	0.11	O	Ala-9
2.19	0.01	O	Ala-20

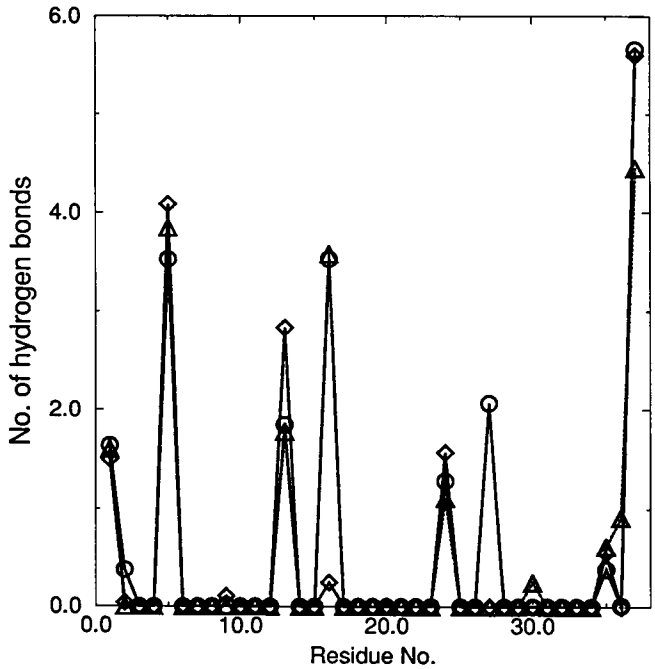

FIGURE 9 Number of hydrogen bonds formed by each residue of the peptides with ice molecules. The circles are for native AFP-ice hydrogen bonds, the triangles are for the S11 mutant, and the squares are for the S23 mutant.

behavior is indicative of clathrate formation around each hydrophobic CH_3 group.

When adsorbed on a neat ice surface, the overall values of the g(r) are reduced significantly because the ice slab does not fill all available space. Here only the relative values and the shape of the g(r) were of concern. The g(r) for CH_3 of Thr-13 (see Fig. 12 *b*) and Thr-24 show features similar to the solvated phase except the peak is shifted to a smaller distance (r = 3.3 Å–3.6 Å *versus* 3.8 Å). This is likely due to the strong hydrogen bonding between the ice surface and the -OH group of these two Thr residues, which "drag" the CH_3 closer to the rigid ice surface. The peak position for $g_{c\text{-}hw}(r)$ is closer than that of $g_{c\text{-}ow}(r)$ and is likely due to the smaller van der Waals radius of the H atom. The calculation also shows that four ice molecules stay within 5 Å of the CH_3 groups of Thr-13 and Thr-24. Two of the water molecules are located in the ridge and two on the step of the ice surface and the CH_3 group sits above these four ice molecules which form a square on the ice surface. The g(r) of the CH_3 of Thr-2 demonstrates that very few ice water molecules are in its vicinity. This is consistent with the binding details of this residue discussed above. The water distribution around the CH_3 of Thr-35 indicates that four ice water molecules stay within 5 Å. However, the water molecules are located in the valley, due to fraying of the C-terminal discussed above.

For the β-branched Leu-12 (see Fig. 12 *c*) and Leu-23 residues in the adsorbed phase, the g(r) for the two CH_3 groups are different from each other. The g(r) results show that there are no ice molecules within the immediate vicinity of one of the CH_3 of the Leu residues. The water distribution around the other CH_3 group shows a pattern similar to the solvated phase except the peak position is at a slightly greater distance (r = 4.2–4.6 Å). This may be related to the fact that the constraints of the backbone or the other CH_3 group prevent this CH_3 group from approaching the valley of the surface. Similarly, for the Ala residues (see Fig. 12 *d*) that directly face the ice surface the g(r) plots are similar to the solvated phase, except the peak position is slightly further away (at r = 4.5 Å compared to r = 3.8 Å in the solvated phase). Again, this is likely related to the constraint of the backbone and the short side chain of Ala. The CH_3 of Ala-9, Ala-20, and one of the CH_3's of Leu-12 and Leu-23 are also in close contact (within 5 Å) with five ice molecules. If one looks down the *z* axis these five water molecules, together with another slightly distant one, form a hexagonal pattern on the surface into the center of which the corresponding CH_3's sit.

Taken together, our results suggest that the ice surface is "pre-organized" to allow for favorable van der Waals interactions of hydrophobic groups with the ice surface. More-

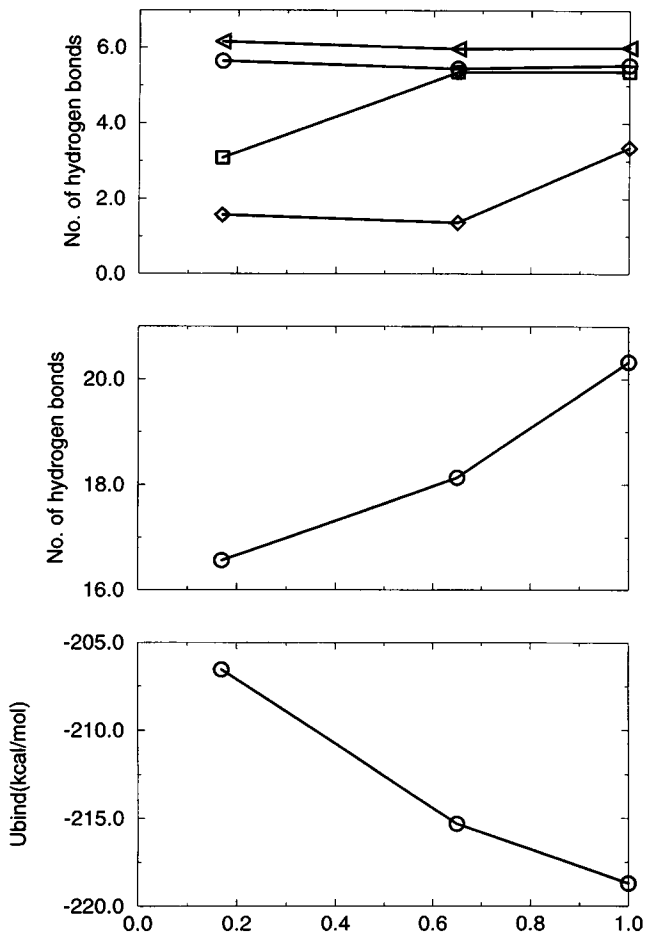

FIGURE 10 The number of hydrogen bonds for each of the four ice-binding groups (*top panel*) as a function of peptide antifreeze activity (S23 0.17, S11 0.65, and native 1.0). The circles, squares, diamonds, and triangles are for binding groups Asp-1/Thr-2/Asp-5, Thr-13/Asn-16 (and its mutated sequence Thr-16/Asn-13 in S23), Thr-24/Asn-27 (and its mutated sequence of Thr-24/Asn-30 in S11 and S23) and Thr-35/Arg-37, respectively. The total number of hydrogen bonds between peptide and ice (*central panel*) and peptide-ice binding energy (*bottom panel*), as a function of antifreeze activity (S23 0.17, S11 0.65, and native 1.0).

over, the ice molecules are already preorganized into a clathratelike shell that reduces the hydrophobic effect penalty expected by the placement of a hydrophobic group near water molecules. Thus, in aqueous solution the AFP peptide experiences an unfavorable hydrophobic effect that leads to clathrate formation and a reduced solvation free energy for the peptide. However, placing the peptide next to a preorganized ice surface where the clathrate formation penalty has already been paid due to the formation of ice reduces the unfavorable hydrophobic effect, thereby enhancing the ice binding propensity of the AFP. There is experimental evidence that this might be the case. For example, the site-directed mutagenesis experiments of Wen and Laursen indicated that the replacement Leu by Ala reduces antifreeze activity by 67% (Wen and Laursen, 1992b). The mutagenesis results allow us to examine the role the hydrophobic effect plays through the use of the following thermodynamic cycle if one assumes that activity and ice binding (i.e., the free energy of binding) are related.

$$\begin{array}{ccc} \text{AFP Leu } (aq) & \xrightarrow{\Delta G(\text{Leu})_{\text{bind}}} & \text{AFP Leu (ice)} \\ \downarrow \Delta G_{\text{sol}} & & \downarrow \Delta G_{\text{ice}} \\ \text{AFP Ala (aq)} & \xrightarrow{\Delta G(\text{Ala})_{\text{bind}}} & \text{AFP Ala (ice)} \end{array}$$

$$\Delta\Delta G_{\text{bind}} = \Delta G(\text{Ala})_{\text{bind}} - \Delta G(\text{Leu})_{\text{bind}} = \Delta G_{\text{ice}} - \Delta G_{\text{sol}}$$

If the hydrophobic effect is operative, then ΔG_{sol} will be more favorable for the Ala mutant than the native AFP with Leu because of the deletion of the hydrophobic alkyl chain. This free energy difference has been estimated to be −0.65 kcal/mol for Leu→Ala (Bash et al., 1987). We also know that the $\Delta\Delta G_{bind}$ for the Leu→Ala mutant has to be positive in order to predict the reduction in the activity of the mutant AFP. If we then use the equation at the bottom of the thermodynamic cycle we can predict what the magnitude of ΔG_{ice} has to be in order to obtain a positive $\Delta\Delta G_{bind}$. If we assume that ΔG_{ice} favors the Ala mutant by a large amount we find that $\Delta\Delta G_{bind}$ can actually take on a negative value, which cannot be the case if we are to rationalize the experimental results. Thus, ΔG_{ice} has to favor the native AFP and take on a positive value in order for $\Delta\Delta G_{bind}$ to be positive. Thus, from this analysis we can see that the relative ice-binding propensity of the native AFP is a combination of favorable van der Waals contacts with the surface as well as an unfavorable hydrophobic effect, which helps drive the AFP to the ice surface in order to reduce this effect. The relative importance of each component is not clear, but it can range from a situation where the hydrophobic effect is dominant in solution (e.g., $\Delta G_{ice} \approx 0.0$) to where it plays a relatively minor role (e.g., $\Delta G_{ice} \gg \Delta G_{sol}$). Determining the values of these two competing factors will be critical in furthering our understanding of how these peptides function. Finally, we note that recent studies on the type III antifreeze protein also suggests that the hydrophobic interactions play an important role in ice-binding (Jia et al., 1996; Sönnichsen et al., 1996). Clearly more study is necessary to clarify what role the hydrophobic effect plays in the binding AFPs to ice.

CONCLUSIONS

We have studied the type I antifreeze protein from winter flounder and two mutants using molecular dynamics simulation techniques. The simulations were performed for the AFP in the gas phase, solvated by water, and adsorbed on the ice (20$\bar{2}$1) crystal plane over relatively long simulation time scales to ensure that the systems were well equilibrated. This study provided unique molecular-level details of the structure of the AFP and its ice-binding pattern.

The simulation results indicated that the AFP and two mutants maintain a stable α-helical structure under all simulation conditions. The average backbone dihedral angles stay within 15° of an ideal α-helix for over 80% of the time.

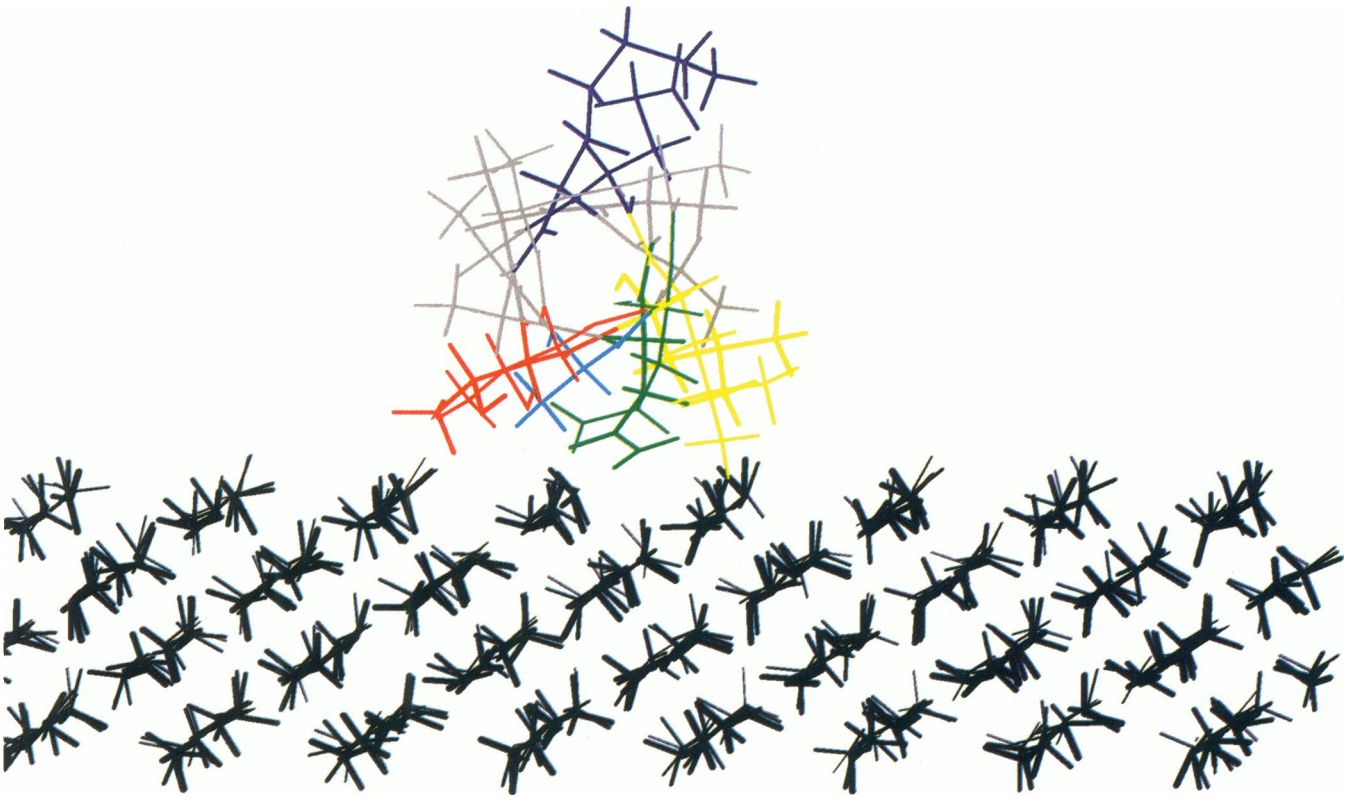

FIGURE 11 A snapshot of the AFP on the ice surface viewed along the helix axis. Here only residues 12 to 27 are shown for clarity. The color code is the same as in Fig. 4 except that Ala-20 is in cyan to show the van der Waals interactions with the surface. This picture shows that the Thr and Asn residues are roughly 60° apart about the helix axis and sit above the ice with a "fork"-like geometry. Ala-20 sits directly above the ice. The side chains of Leu-12 and Leu-23 also interact with the surface through van der Waals interaction.

The backbone hydrogen bonds, formed by the carbonyl oxygen atoms and the amide hydrogen atoms of the fourth residue, are very stable, except at the C- and N-terminal regions of the helix. Some hydrogen atoms on the side chains also form hydrogen bonds with atoms on the neighboring residues. Both the N- and C-termini are partially frayed; however, they are capped by hydrogen bond networks formed by the flanking residues in the gas and adsorbed systems. This observation agrees with a recent experimental study (Sicheri and Yang, 1995). A salt bridge was formed in the gas and adsorbed phase between Lys-18 and Glu-22, but this interaction was lost in the solvated systems. When solvated by water, most charged and some of the polar side chains extended into water to form hydrogen bonds, thereby reducing the intrapeptide hydrogen bonding as well as breaking the cap structure at the C- and N-termini. The side chain torsion angles of the 14 non-Ala residues were also examined. The side chains of Asp and Asn show great flexibility in the gas and solvated phase, but become rigid when adsorbed on the ice surface, since they are pinned to the surface via hydrogen bonding. The side chain -OH group of the Thr residues are rigid because the hydrogen atoms are hydrogen-bound to the backbone carbonyl oxygen of the Ala residues. The $-CH_3$ group of the Thr residues appears to be rigid due to steric constraints.

The hydrogen bonds formed between the AFP and water molecules, when solvated or adsorbed on ice, are, not unexpectedly, mostly between the charged or polar side chains and water. Nevertheless, almost all carbonyl oxygen atoms hydrogen bond weakly to water. When adsorbed on the ice surface, only charged and polar side chains (except Ser-4, Lys-18, and Glu-22) hydrogen-bond to the ice water molecules.

The most striking result is the detailed picture of the ice binding pattern observed here. Indeed, the helix aligns along $\langle \bar{1}102 \rangle$ axis of the ice surface, which is in agreement with the experimental results (Knight et al., 1991). Both the Thr and Asx residues are evenly spaced along the α-helix and the distance between neighboring pairs of Thr or Asx residues matches the ice lattice spacing of the $\langle \bar{1}102 \rangle$ direction within 2 Å. The ice-binding atoms are clearly located in four regions and are from Thr, Asx, and Arg. They can be divided into four binding groups or regions that are composed of Asp-1/Thr-2/Asp-5, Thr-13/Asn-16, Thr-24/Asn-27, and Thr-35/Arg-37. The average number of hydrogen bonds each group contributes in the neat adsorbed system are 5.5, 5.4, 3.3, and 6.0, respectively. The location of these four ice-binding groups matches the $\langle \bar{1}102 \rangle$ lattice spacing well.

The Thr and Asx residues within a group are three residues apart, which is not enough to complete a full turn. The

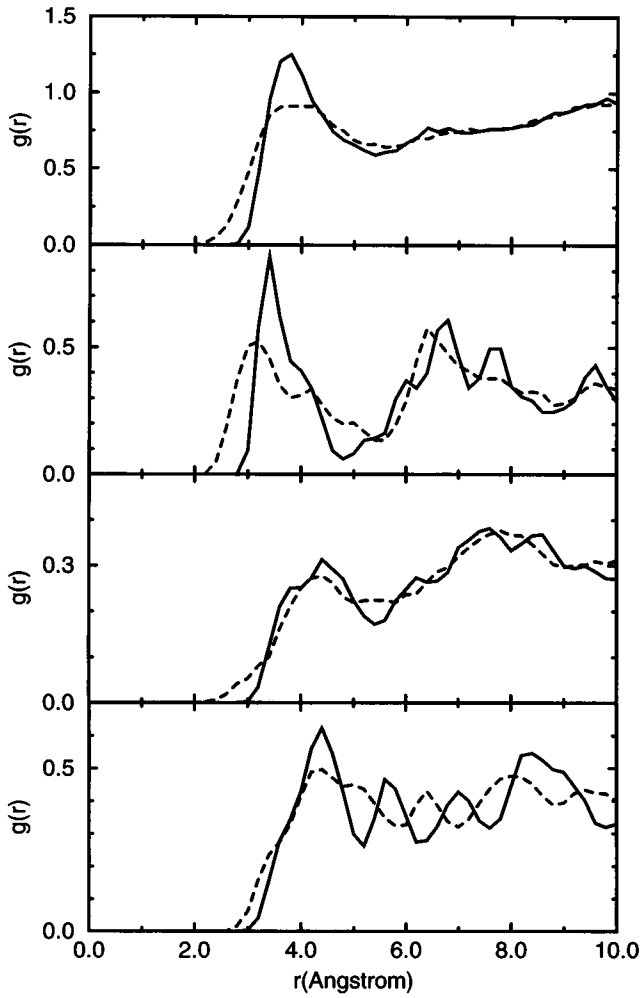

FIGURE 12 The water radial distribution function, g(r), around the methyl carbon atoms of selected residues in the solvated and pure adsorbed phases. From top to bottom we present: (*a*) Thr-13 in the solvated phase; (*b*) Thr-13 in the adsorbed phase; (*c*) Leu-12 (one of the two CH_3) in the adsorbed phase; (*d*) Ala-9 in the adsorbed phase. The solid lines are for the oxygen atom of water and the dashed lines are for the hydrogen atoms of water. The positions of the first peak for OW and OH are the same in (*a*), (*c*), and (*d*). This suggests that a clathrate-like structure is formed on the ice surface for these groups.

two residues are 60° apart about the helix axis and, therefore, both can face the ice surface simultaneously. The ice surface that is complementary to the AFP has what can be termed a ridge/step/valley topology (see Figs. 5 and 6). We have found that Asx residues typically hydrogen-bond to three water molecules located on the step of the ice surface (e.g., 3.5 hydrogen bonds for Asp-5 and Asn-16, and 2 hydrogen bonds for Asn-27). Thr residues hydrogen-bond to 2 water molecules on the ice surface ridge with a total of 1.5 hydrogen bonds. It is clear that Asx and Arg form more than twice as many hydrogen bonds as Thr with the surface, thus playing an important role in ice binding. This finding agrees with the proposed model by Wen and Laursen (1992a; 1993); however, it disagrees with the MD simulation study by Jorgensen et al. (1993). Their results suggested that all charged residues stay on one side of the helix and Thr residues stay on the opposite side. Thus, the former residues do not participate in the ice binding.

The distance between the corresponding backbone atoms of Thr and Asx within the same group was found to be 4.9 Å, while that between the ice-binding atoms was 6–8 Å. The vector connecting the two residues intersects the helix axis by 20–30°, and was not parallel to the ridge/valley orientation, which is along the ⟨010⟩ direction. This result does not support the proposed alignment based on an x-ray study (Sicheri and Yang, 1995).

The results from the two mutants suggests that both the correct Thr-Asn distance and ordering are crucial to ice binding. Since the hydrogen bonding capabilities and steric "signature" of Thr and Asn are different, it is critical to have these residues arrayed along the peptide sequence such that a binding surface is generated that presents the maximum number of hydrogen-bonding opportunities while being sterically complementary to the ice surface, and meanwhile maximize the nonhydrogen bond interactions between AFP and ice surface. Therefore, the peptide atoms may occupy the vacant ice lattice sites to form a stable hydrogen bond network. However, when the sequence is altered we find that the ice/peptide complementarity is reduced, which results in the decreased activity of the mutant peptides to the native peptide.

We also note that the number of hydrogen bonds estimated here is greater than that reported by Wen and Laursen (1992a). This is likely due to the difference in the methods used in the two studies. Wen and Laursen used energy minimization techniques, which implies that the structure is at 0 K. This work was carried out using molecular dynamics simulation at 300 K. Thus, it is clear that through the use of MD simulations we have been able to sample the peptide/ice potential energy more thoroughly, resulting in a better interaction between the peptide and the ice surface.

The hydrophobic side chains of Ala-9, Leu-12, Ala-20, and Leu-23 point into the valley of the surface and facilitate the ice binding by maximizing favorable van der Waals interactions. The methyl groups of Thr side chains also orient toward the surface step and enhance the binding though van der Waals interactions. Furthermore, we propose that the hydrophobic effect may also play a key role in ice-binding because the ice surface is preorganized (i.e., preformed clathrate shells) in such a way to minimize the effect of placing a nonpolar group near water molecules. The relative importance of van der Waals interaction versus the hydrophobic effect is unknown at this time, but should be the attention of future computational and experimental studies. One can also take the advantage of the MD technique to predict the activity of new mutants, thus to design better antifreeze proteins.

This work has provided molecular-level details regarding ice binding of the AFP peptide. It seems all residues play an important role either in ice-binding or helix stabilization. We find that the Arg and the evenly spaced Thr and Asx residues are responsible for the ice-binding because, most

importantly, these residues match the lattice spacing and topology of the ice surface.

We thank the Pittsburgh Supercomputer Center and the Cornell Theory Center for generous allocations of parallel computer time through a Meta-Center grant.

This work was supported by the Office of Naval Research through Grant N00014-93-1-0887.

REFERENCES

Ananthanarayanan, V. A. 1989. Antifreeze proteins: structural diversity and mechanism of action. *Life Chem. Rep.* 7:1–32.

Arav, A., B. Rubinsky, G. Fletcher, and E. Seren. 1993. Cryogenic protection of oocytes with antifreeze proteins. *Mol. Reprod. Dev.* 36: 488–493.

Bash, P. A., U. C. Singh, R. Langridge, and P. A. Kollman. 1987. Free energy calculations by computer simulation. *Science (Washington).* 236: 564–568.

Berendsen, H. J. C., J. P. M. Postma, W. F. v. Gunsteren, A. DiNola, and J. R. Haak. 1984. Molecular dynamics with coupling to external bath. *J. Chem. Phys.* 81:3684–3690.

Burcham, T. S., D. T. Osuga, H. Chino, and R. E. Feeney. 1984. Analysis of antifreeze glycoproteins in fish serum. *Anal. Biochem.* 139:197–204.

Chakrabartty, A., V. S. Ananthanarayanan, and C. L. Hew. 1989a. Structure-function relationships in the winter flounder antifreeze polypeptide I. *J. Biol. Chem.* 264:11307–11312.

Chakrabartty, A., D. S. C. Yang, and C. L. Hew. 1989b. Structure-function relationship in a winter flounder antifreeze polypeptide II. *J. Biol. Chem.* 264:11313–11316.

Cheng, A., and K. M. Merz, Jr. 1996. Application of the Nosé-Hoover chain algorithm to the study of protein dynamics. *J. Phys. Chem.* 100:1927–1937.

Chou, K.-C. 1992. Energy-optimized structure of antifreeze protein and its binding mechanism. *J. Mol. Biol.* 223:509–517.

Creighton, T. E. 1993. Protein Structures and Molecular Properties. W. H. Freeman and Company, New York.

Davies, P. L., and C. L. Hew. 1990. Biochemistry of fish antifreeze proteins. *FASEB J.* 4:2460–2468.

DeVries, A. L., S. K. Komatsu, and R. E. Feeney. 1970. Chemical and physical properties of freezing point-depressing glycoproteins from antarctic fishes. *J. Biol. Chem.* 245:2901–2908.

Feeney, R. E., T. S. Burcham, and Y. Yeh. 1986. Antifreeze glycoproteins from polar fish blood. *Annu. Rev. Biophys. Biophys. Chem.* 15:59–78.

Feeney, R. E., and Y. Yeh. 1993. Antifreeze proteins: properties, mechanism of action, and possible applications. *Food Technol.* Jan.:82–89.

Hansen, T. N., and J. F. Carpenter. 1993. Calorimetric determination of inhibition of ice crystal growth by antifreeze protein in hydroxyethyl starch solutions. *Biophys. J.* 64:1843–1850.

Hays, L. M., R. E. Feeney, L. M. Crowe, and J. H. Crowe. 1993. Interaction of antifreeze glycoproteins with liposomes. *Biophys. J.* 64:296*a* (Abstr.).

Hew, C. L., C. L. Wang, S. Yan, H. Cai, A. Sclater, and G. L. Fletcher. 1986. Biosynthesis of antifreeze polypeptides in the winter flounder characterization and seasonal occurrence of precursor polypeptides. *Eur. J. Biochem.* 160:267–272.

Jia, Z., C. I. DeLuca, H. Chao, and P. L. Davies. 1996. Structural basis for the binding of a globular antifreeze protein to ice. *Nature.* 384:285–288.

Jorgensen, H., H. Matsui, M. Kanaoka, H. Yanagi, Y. Yabussaki, and Y. Kikuzono. 1993. Molecular dynamics simulations of winter flounder antifreeze protein variants in solution: correlation between side chain spacing and ice lattice. *Protein Engin.* 6:19–27.

Jorgensen, W. L., J. Chandrasekhar, J. D. Madura, R. W. Impey, and M. L. Klein. 1983. Comparison of simple potential functions for simulating liquid water. *J. Chem. Phys.* 79:926–935.

Karim, O. A., and A. D. J. Haymet. 1988. The ice/water interface: a molecular dynamics simulation study. *J. Chem. Phys.* 89:6889–6896.

Kenward, K. D., M. Altschuler, D. Hildebrand, and P. L. Davies. 1993. Accumulation of type I fish antifreeze protein in transgenic tobacco is cold-specific. *Plant Mol. Biol.* 23:377–385.

Kerr, W. L., D. T. Osuga, R. E. Feeney, and Y. Yeh. 1987. Effects of antifreeze glycoproteins on linear crystallization velocities of ice. *J. Cryst. Growth.* 85:449–452.

Knight, C. A., C. C. Cheng, and A. L. DeVries. 1991. Adsorption of α-helical antifreeze peptides on specific ice crystal surface planes. *Biophys. J.* 59:409–418.

Knight, C. A., A. L. DeVries, and L. D. Oolman. 1984. Fish antifreeze protein and the freezing and recrystallization of ice. *Nature.* 308: 295–296.

Lal, M., A. H. Clark, A. Lips, J. N. Ruddock, and D. N. J. White. 1993. Inhibition of ice crystal growth by preferential peptide adsorption: a molecular dynamics study. *Faraday Discuss.* 95:299–306.

Madura, J. D., A. Wierzbicki, J. P. Harrington, R. H. Maughon, J. A. Raymond, and C. S. Sikes. 1994. Interactions of the D- and L-forms of winter flounder antifreeze peptide with the {201} planes of ice. *J. Am. Chem. Soc.* 116:417–418.

McDonald, S. M., J. W. Brady, and P. Clancy. 1993. Molecular dynamics simulations of a winter flounder "antifreeze" polypeptide in aqueous solution. *Biopolymers.* 33:1481–1503.

Myers, J. K., and C. N. Pace. 1996. Hydrogen bonding stabilizes globular proteins. *Biophys. J.* 71:2033–2039.

Pain, R. H. 1988. Helices of antifreeze. *Nature.* 333:207–208.

Pearlman, D. A., D. A. Case, J. C. Caldwell, G. L. Seibel, U. C. Singh, P. Weiner, and P. A. Kollman. 1991. AMBER 4.0. University of California, San Francisco.

Raymond, J. A., and A. L. DeVries. 1977. Adsorption inhibition as a mechanism of freezing resistance in polar fishes. *Proc. Natl. Acad. Sci. USA.* 74:2589–2593.

Rossky, P. J., and M. Karplus. 1979. Solvation. A molecular dynamics study of a dipeptide in water. *J. Am. Chem. Soc.* 101:1913–1937.

Ryckaert, J. P., G. Ciccotti, and H. J. C. Berendsen. 1977. Numerical integration of the cartesian equations of motion of a system with constraints: molecular dynamics of *n*-alkanes. *J. Comput. Phys.* 23: 327–341.

Sicheri, F., and D. S. C. Yang. 1995. Ice-binding structure and mechanism of an antifreeze protein from winter flounder. *Nature.* 375:427–431.

Sönnichsen, F. D., C. I. DeLuca, P. L. Davies, and B. D. Sykes. 1996. Refined solution structure of type III antifreeze protein: hydrophobic groups may be involved in the energetics of the protein-ice interaction. *Structure.* 4:1325–1337.

Swaminathan, S., S. W. Harrison, and D. L. Bereridge. 1978. Monte Carlo studies on the structure of a dilute aqueous solution of methane. *J. Am. Chem. Soc.* 100:5705–5712.

Teeter, M. M. 1984. Water structure of a hydrophobic protein at atomic resolution: pentagon rings of water molecules in crystals of crambin. *Proc. Natl. Acad. Sci. USA.* 81:6014–6018.

Tirado-Rives, J., and W. L. Jorgensen. 1990. Molecular dynamics of protein with the OPLS potential functions. Simulation of the third domain of silver pheasant ovomucoid in water. *J. Am. Chem. Soc.* 112: 2773–2781.

Weiner, S. J., P. A. Kollman, D. A. Case, U. C. Singh, C. Ghio, G. Alagona, J. S. Profeta, and P. Weiner. 1984. A new force field for molecular mechanical simulation of nucleic acids and proteins. *J. Am. Chem. Soc.* 106:765–784.

Wen, D., and R. A. Laursen. 1992a. A model for binding of an antifreeze polypepetide to ice. *Biophys. J.* 63:1659–1662.

Wen, D., and R. A. Laursen. 1992b. Structure-function relationship in an antifreeze polypeptide. *J. Biol. Chem.* 267:14102–14108.

Wen, D., and R. A. Laursen. 1993. A D-antifreeze polypeptide displays the same activity as its natural L-enantiomer. *FEBS Lett.* 317:31–34.

Wyckoff, R. W. G. 1969. Crystal Structures. Interscience Publishers, New York.

Yang, D. S. C., M. Sax, A. Chakrabartty, and C. L. Hew. 1988. Crystal structure of an antifreeze polypeptide and its mechanistic implications. *Nature.* 333:232–237.

Yeh, Y., and R. E. Feeney. 1996. Antifreeze proteins: structures and mechanism of function. *Chem. Rev.* 96:601–617.